T2R2 東京科学大学 リサーチリポジトリ
Science Tokyo Research Repository

論文 / 著書情報
Article / Book Information

題目(和文)	歩行のための皮質電流源推定に基づく脳信号デコーダ
Title(English)	A Brain-signal Decoder Based on Cortical Current Source Estimation for Walking
著者(和文)	MejiaT. Alejandra
Author(English)	Alejandra Mejia Tobar
出典(和文)	学位:博士(学術), 学位授与機関:東京工業大学, 報告番号:甲第11008号, 授与年月日:2018年9月20日, 学位の種別:課程博士, 審査員:吉村 奈津江,小池 康晴,熊澤 逸夫,中村 健太郎,金子 寛彦
Citation(English)	Degree:Doctor (Academic), Conferring organization: Tokyo Institute of Technology, Report number:甲第11008号, Conferred date:2018/9/20, Degree Type:Course doctor, Examiner:,,,,
学位種別(和文)	博士論文
Type(English)	Doctoral Thesis

Powered by T2R2 (Science Tokyo Research Repository)

東京工業大学
Tokyo Institute of Technology

A brain-signal decoder based on cortical current source estimation for walking

Doctoral Thesis by:
Alejandra Mejia Tobar

Supervised by:
Professor Natsue Yoshimura
Professor Yasuharu Koike

Koike – Yoshimura Laboratory
Interdisciplinary Graduate School of Science and Engineering
Department of Information Processing
Tokyo Institute of Technology
2018

Acknowledgements

I would like to express my deepest gratitude to my supervisors, Professor Natsue Yoshimura and Professor Yasuharu Koike, for their kind guidance and support throughout my graduate courses in Tokyo Institute of Technology. Beyond their excellent academic guidance, I found personal strength and growth in their teaching.

Also, I would like to thank the ACLS program for enriching my professional career by shaping me into a gamma-type professional, and for their financial support.

Last but not least, I would like to thank my parents, my brothers and my husband who have always believed in me, and who have made the utmost effort to give me the opportunity to excel in Japan and in my career.

Table of Contents

Abstract

Persons with walking impairments often rely on the remaining motor function in the upper limbs in order to control assistive devices for transportation. While these devices accomplish their function, the activities of daily living that the user can perform are reduced. Well-established transportation systems such as wheelchairs, are widely available and provide the simplest way of transportation, however its use has some drawbacks that include limited accessibility in some public spaces and pressure soars that may require hospitalization in the long term. Alternatives to wheelchairs such as exoskeleton (robotic frames attached to the legs), and neuroprostheses (defined in this context as electrical stimulation of muscles and peripheral nerves) allow its users to stand up and take steps. These systems usually detect trunk shifts or direct commands from controllers placed on crutches to trigger a walking sequence. While exoskeletons and neuroprosthesis for walking are improved transportation aids that have physical and psychological benefits for its users, its control still requires the use of the remaining motor functions. As an alternative for these control approaches, brain-computer interfaces (BCI), systems that acquire brain signals and translate them into commands for machines, are being constantly studied. Research in BCIs applied to exoskeletons and neuroprosthesis, has been focused towards detecting walking intention to trigger the gait sequence, aiming to give the user more intuitive control and freedom when using these devices.

Brain signal acquisition for BCIs is done with invasive and non-invasive recording methods. In invasive methods, surgery is required to place electrodes over a small area in the exposed cerebral cortex. This recording method is known as electrocorticography (ECoG) and it provides electrophysiological recordings with high spatial and high temporal resolution. On the other hand, non-invasive methods for BCIs include mainly electroencephalography (EEG), which is recorded from electrodes placed over the scalp. EEG has a high temporal resolution, but a poor spatial resolution because neural signals are largely dispersed by the time they reach the scalp. EEG is portable and easy to set up, which makes them favorite for BCI implementations. BCIs based on ECoG can achieve precise control of robots, while BCIs based on EEG are mostly used for the detection of movement intention (binary decoding) since the limited spatial resolution makes it difficult to discriminate motor functions concentrated over small regions of the brain. Such is the example of walking, where the brain areas responsible for the left and right legs are located closely to one another in the motor cortex, making it difficult to detect various lower limbs movements separately. Some studies have performed multi class decoding of motor imagery of different parts of the body, but the multi class decoding of various walking-related motor tasks from EEG, is still an emerging field.

This research is aimed to design a brain-signal decoder for walking that can detect multiple motor tasks instead of only movement intention. Multi-class decoding will allow for the design of more natural and intuitive brain-computer interfaces. To achieve this objective, a methodology that combines cortical current source estimation using a hierarchical variational Bayesian estimation method (VBMEG) and a sparse logistic regression for multi-class classification is proposed. By using these methods, it is possible to combine the high spatial resolution of functional magnetic resonance imaging (fMRI) and EEG, to estimate hundreds or up to thousands of current sources relevant to walking tasks. The walking tasks selected in this study for the experiments are ankle flexion and extension at two force levels, since these are fundamental movements in the normal walking cycle.

The first and second chapters introduce about walking impairments, brain computer interfaces, the methods used for source estimation and classification, and signal preprocessing.

The third chapter is focused on the decoding of ankle flexion and extension, using current sources estimated from well-known areas in the brain that are related to motor planning and execution. fMRI is used to obtain area and activity priors, to estimate cortical current sources from the EEG recordings. Nine-class classification is done with a sparse logistic regression for current sources and for processed EEG sensor signals. Finally, a weight analysis of selected vertices by the classifier is performed.

In the fourth chapter, the feasibility of reducing the number of used EEG electrodes is discussed. Since this work is focused to provide an insight of design for a BCI for walking, the relationship between the number of EEG electrodes and the classification accuracies is studied, to determine the minimum number of electrodes that can provide a good classification accuracy. Additionally, in this analysis area and activity priors are not used, and current sources are estimated over the whole cortex of the brain model.

Chapter 1: Introduction

1.1. Walking impairments

Paralysis can be defined as the loss of motor control on a body part. The causes of paralysis involve traumatic injuries, diseases of the nervous system and congenital conditions that affect the brain, the spinal cord and/or the muscles. The type of paralysis depends on the parts of the body affected, and the level of remaining sensation and/or motor control in those parts. In line with the title and objective of this manuscript, we will refer only to two main types of paralysis affecting the normal walking cycle in humans: hemiplegia caused by stroke, and paraplegia caused by spinal cord injury.

Hemiplegia

Hemiplegia is the type of paralysis that affects one side of the body. It is common to find in literature the terms hemiplegia and hemiparesis used indistinctively, however hemiparesis refers to the loss of sensation (or weakness) in one side of the body, while hemiplegia more commonly refers to severe motor loss resulting in the need of aids for mobility.

Among the causes of hemiplegia, stroke is one of the most common causes. A stroke happens when the normal blood flow to the brain is interrupted either by a bleeding (hemorrhagic stroke), or to an interruption of blood supply due to a blood clot blocking a blood vessel in the brain (ischemic stroke). As a result of the decrease in the blood flow, the brain cells in the affected area begin to die due to the lack of oxygen and nutrients. Consequently, the motor functions controlled by that part of the brain, are partially or completely lost in the contralateral side of the body.

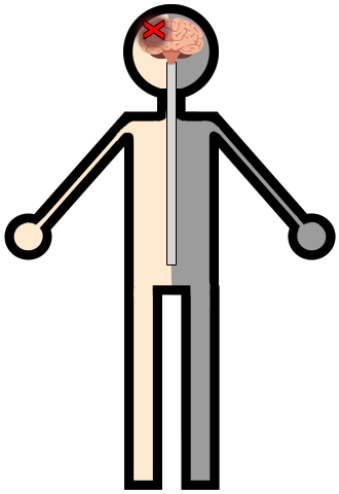

Figure 1 – Hemiplegia. A lesion in the brain results in the loss or reduction of sensation and motor control in the body parts contralateral to area of the brain affected.

Paraplegia

Paraplegia is the condition in which an injury to the spinal cord results in the partial or complete loss of sensation and motor control. The causes of spinal cord injuries include congenital conditions, infections and trauma, being the last one the most prevalent cause. A spinal cord injury affects the motor functions of both sides of the body below the level of the injury. For example, a complete lesion in the 6th thoracic vertebrae (T6) most likely will result in the loss of sensation below T6 and the loss of the ability to walk.

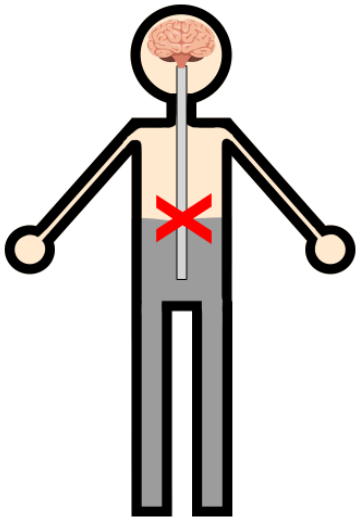

Figure 2 – An injury in the spinal cord results in the complete or partial loss of sensation and motor control, in the body parts located below the level of the injury.

1.2. Current assistive devices for walking

Wheelchairs

Wheelchairs are widely used systems for transportation for patients with walking impairments, however wheelchairs are limited in terms of mobility, and improvement of the physical and mental wellbeing of its users. While wheelchairs accomplish their main objective as transportation systems, its functionality is largely affected depending on the conditions of surrounding areas and terrains. Such is the case for public mobility where alternatives to stairs or escalators are not always available. The use of a wheelchair affects the perception that able-bodied people have about its users, and while not explicitly expressed, wheelchair users are aware of those negative attitudes (Furnham, et al., 1994; Galli, et al., 2015). Finally, some users adapt well to the use of the wheelchair and develop a sense of embodiment (Pazzaglia, et al., 2016), where the wheelchair is felt like a part of the own body, however the users are not always aware of performing pressure-relieving movements frequently and, in the long term, this can result in pressure soars that may require hospitalization (Stockon, et al., 2002).

Due to the limitations of wheelchairs, alternatives for mobility for patients with walking impairments are constantly being researched and developed. Such is the case of functional electrical stimulators and exoskeletons that will be discussed in the following sections.

Functional Electrical Stimulation for Walking

A functional electrical stimulation for walking (FES system), applies bursts of electrical current to the muscles, in order to elicit contractions in a sequence that follows the normal walking (gait) cycle in humans.

The normal gait cycle can be broadly divided into two periods, and more specifically into three tasks. The periods correspond to the “swing” and “stance”, and the tasks to “weight acceptance”, “single limb support” and “limb advancement” as described by Perry et al. Following the movement of the left foot as a reference, the “swing” period is the time when the left foot is in the air, for limb advancement, and the “stance” period is when the left foot is back on the ground. The “weight acceptance” task covers the moment when the left heel touches the ground, to the moment the body weight is transferred from the right foot to the left foot. During the “single limb support” task, the right foot goes into the swing period while the left foot supports the whole body weight. This task ends when the right foot touches the floor again. The “limb advancement” task starts with the left foot going into the swing period and ends when the foot touches the floor again (Perry, 1992).

To detect a specific gait task, period or phase, an FES system for walking may use sensors placed along the legs and/or pressure sensors placed on the shoe sole, to trigger a stimulation sequence in the leg muscles that follow the gait cycle pattern (Negård, et al., 2016). These stimulation sequences can be based on known muscle synergies used by healthy muscles during the gait cycle (Ferrante, et al., 2016).

The purpose of applying FES to patients with walking impairments is to replace lost voluntary muscle contractions (Meng, et al., 2017). In contrast with the exclusive use of wheelchairs, in which muscle atrophy (loss of muscle tissue) due to disuse is a constant concern, FES contributes to improving the patient’s health by increasing the muscle tone (Baldi, et al., 1998; Carraro, et al., 2015; Boncompagni, et al., 2012) and enhancing the brain plasticity in patients affected by stroke (Weingarden, et al., 2006). However, FES will benefit mostly patients with intact lower motor neuron (nerves connecting the spinal cord to the muscles), because their muscles are responsive to electrical stimulation, while patients with lower motor neuron lesion will most likely have flaccid muscles unresponsive to the stimulation.

While FES is not a viable option for patients with lower motor neuron lesion, alternatives like robotic exoskeletons offer these patients the assistance to stand up and take steps.

Exoskeletons

In the context of this study, exoskeletons are defined as external robotic frames that incorporate motor joints in the ankles, knees and/or hips, and assist its users in standing up and taking steps, for physical rehabilitation or daily life. Amongst the most notable recent developments in exoskeletons for walking, the systems Indego (Parker Hannafin, http://www.indego.com/indego/en/home), EksoGT (Ekso Bionics, https://eksobionics.com/eksohealth/products/), PhoeniX (US Bionics, http://www.suitx.com/phoenix), ReWalk (ReWalk Robotics, http://rewalk.com/rewalk-personal-3/) and REX P (REX Bionics, https://www.rexbionics.com/) are found. These systems are usually controlled by trunk shifts (changes in the center of gravity of the body) to initiate walking sequences, and require the use of crutches to assist in standing up and keeping balance, with the exception of the REX P system which does not need crutches, and instead integrates handles with controllers for standing, walking, and turning right and left functions.

While the exoskeletons for walking well achieve their goal in assisting with walking functions in a wide range of paralyses types, these systems are often based on pre-established gait sequences and speeds that may not be fully comfortable or adaptable to a patient. Ideally, a system that can adapt more naturally to its user' intention will be desirable. Such system might be achieved by non-invasively measuring electrophysiological signals, from which we could predict specific movements intentions.

1.3. Brain-Computer Interfaces

The remaining motor control in patients with paralysis is a rich source of information for controlling prosthesis, exoskeletons and FES systems however, depending on the level of the paralysis, it may be difficult for a patient to perform single tasks, such as shifting their trunk to control an exoskeleton, or to use their hands to hold the crutches and keep balance while using an FES system for walking. To further overcome these limitations, the brain signals arising from the execution (or intention) of movements, can be used to generate control commands for exoskeletons or FES systems. This would reduce the need of using the residual motor output, and would increase the activities of daily living the users can perform while on the devices.

Both types of patients affected by a stroke or a spinal cord injury, can produce brain signals containing information related to motor planning and execution. A stroke affects differently each patient since the motor skill affected depends directly on the part of the brain damaged, for example, a stroke that has affected the left hemisphere of the brain over the motor cortex, can cause a decrease or loss of the motor function in the right side of the body. However, to compensate for the loss of a motor function, the brain goes through a

neuroplasticity process, in which the healthy brain areas reorganize to form new synapses (Li, 2017).

In the case of patients with spinal cord injury, the brain most likely remains intact: motor commands are generated and sent from the brain, however these commands cannot reach the peripheral nerves needed to finally elicit muscle contraction and limb movement.

In this sense, both patients with stroke or spinal cord injury are still able to generate motor commands in the brain and the consequent brain activity can be measured.

1.3.1. Introduction to Brain-Computer Interfaces

A brain-computer interface (BCI), or a brain machine interface (BMI), is a system that measures activity directly from the brain, processes the acquired signals and finally translates them into commands to control a device (Wolpaw et al., 2002, 2009). In order to achieve proper BCI control, a BCI user must train to learn to modulate their brain rhythms to elicit the intended response from the BCI every time.

BCIs have a wide range of applications that range from health to entertainment, and are applicable to almost any person. The applications of BCI include the control of neuroprosthesis (prosthesis based on FES), games, spellers, etc. Each of these applications uses different techniques to extract features from the brain activity related to a stimulus or to an intended task.

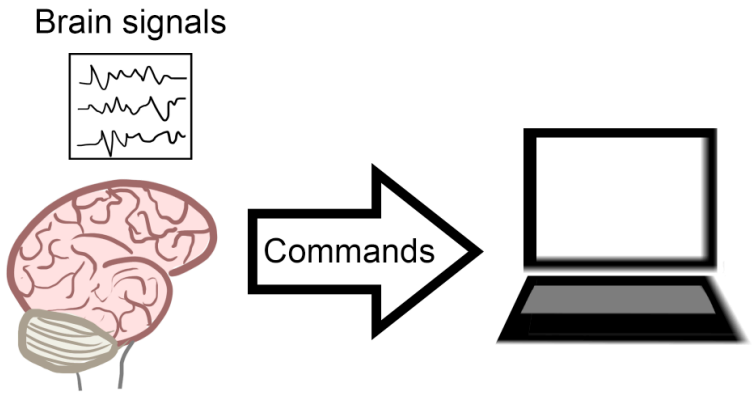

Figure 3 – Diagram of a brain-computer interface

1.3.2. Types of Brain-Computer Interfaces

Although there are several applications of BCIs, these interfaces can be broadly divided into two categories: BCIs for communication and BCIs for control.

BCIS for Communication

These interfaces are oriented for patients with severe neuromuscular paralysis, as in the case of locked-in patients that have complete loss of voluntary muscle control and are unable to communicate in any way (Wolpaw, et al., 2002). BCIs for spelling are interfaces that use a grid of letters on a screen, to spell words based on brain signal arising from the intention of the user. BCIs for spelling are divided into two categories: reactive and active BCI spellers. Reactive spellers use brain signals that arise as a response to external stimuli such as infrequently presented images or sounds (P300 potentials), and active spellers use brain rhythms arising from the BCI user intention without any external stimuli (Zander, et al., 2009).

BCIs for Control

These are BCIs that take brain signals arising from actual motor execution, or movement intention (motor imagery), to control any system that assists in movement control, for example, exoskeletons for walking, arm prosthesis, neuroprosthesis, etc.

The first breakthroughs in BCI for motor control were done using implanted electrodes placed on the brain cortex. Some of the most notable names include Nicolelis, Schwartz and Donoghue. Nicolelis developed BCIs to control robots for reaching and grasping in primates (Wessberg, et al., 2000; Carmena, et al., 2003). Schwartz' BCI achieved control of a prosthetic arm for self-feeding (Taylor et al., 2002; Velliste, et al., 2008), and Donoghue developed a BCI that allowed a patient with paraplegia to control a prosthesis for reaching and grasping (Hochberg, et al., 2012) .

Due to the complexity of placing electrodes on the cortex of the brain, developments based on non-invasive brain signal recordings started to emerge. Several developments have been done for BCIs for walking, including the recent breakthrough of Nicolelis in the 2014 World Cup (http://virtualreality.duke.edu/project/walk-again-project/) and other notable recent developments available in (Fitzsimmons, 2009; Xu, et al., 2014; King, et al., 2015; Jiang, et al., 2015; Severens, et al., 2015; Pereira, et al., 2017).

1.4. Brain Activity Recording Methods

Techniques for acquiring brain signals are divided into two types: invasive and non-invasive. The invasive technique includes the electrocorticography (ECoG) and the non-invasive techniques include electroencephalography (EEG), magnetoencephalography (MEG) and functional magnetic resonance imaging (fMRI).

ECoG

The monitoring of brain signals using ECoG is performed with an array of electrodes placed directly over the exposed cerebral cortex. These type of recordings provide the highest

spatial (~ 1cm) and temporal (≥5ms) resolution, however the placement of these electrodes require surgery, and therefore the population that can access to this technique is greatly limited due to the inherent risks of surgery.

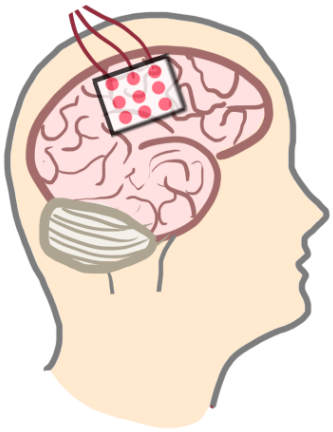

Figure 4 – EcoG electrode placement

MEG

MEG measures the magnetic field generated by electrical currents resulting from post-synaptic current flows. This technique has a spatial and temporal resolution comparable to ECoG (Singh, 2014), however MEG acquisitions systems are bulky and require special rooms for their setting, therefore MEG is not suitable for out-of-laboratory BCIs.

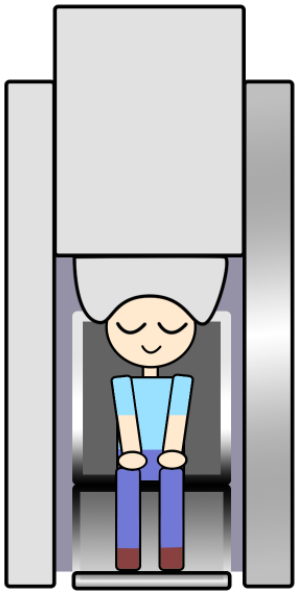

Figure 5 – MEG Machine

fMRI

Magnetic resonance imaging (MRI) is a technique that uses magnetic fields and radio frequency to temporarily modify the spin of the hydrogen nuclei (contained in the water molecules in the human body). The MRI machine measures the radio signal produced when

the nuclei return to their natural orientation. This signals are used then to produce high-resolution images.

fMRI is based on the MRI principle, however fMRI measures the ratio of oxygenated/deoxygenated blood: In theory, an active brain area requires higher levels (than baseline) of oxygenated hemoglobin. Right after the neural activity, the ratio of oxygenated-deoxygenated blood decreases. To compensate, more oxygenated hemoglobin is rushed to the active brain area, and the ratio of oxygenated-deoxygenated blood rapidly increases. This ratio is known as the blood oxygen-level dependent (BOLD) signal. Since fMRI measures a ratio of oxygenated blood, it is considered an indirect measure of neural activity (Ashby, 2011).

fMRI has a high spatial resolution of 3-5 mm^3 and a low temporal resolution of 1-3 seconds, however MRI scanners are big and require a special room for their setting, therefore are not suitable for portable BCI applications.

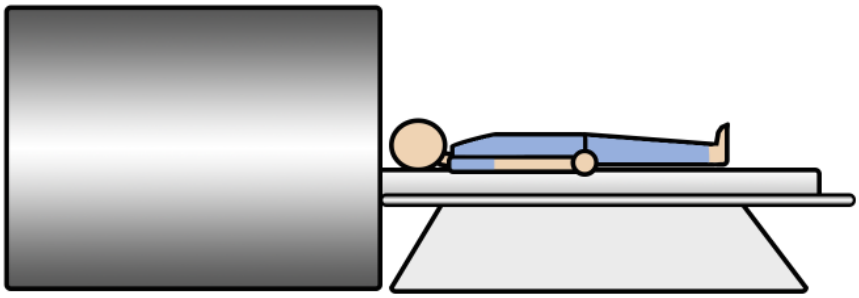

Figure 6 – MRI Scanner

EEG

EEG systems are composed by arrangement of electrodes placed over the scalp measuring neural activity. Due to the conductive properties of the skull and the scalp, the signals generated in the brain are largely attenuated by the time they reach the EEG electrodes. For this reason, EEG measures the electrical activity generated by large populations of neuron, hence the low spatial resolution of EEG. EEG has a high temporal resolution and it is relatively not demanding regarding experimental setting and use. The EEG systems are portable and its use is preferable for BCI applications.

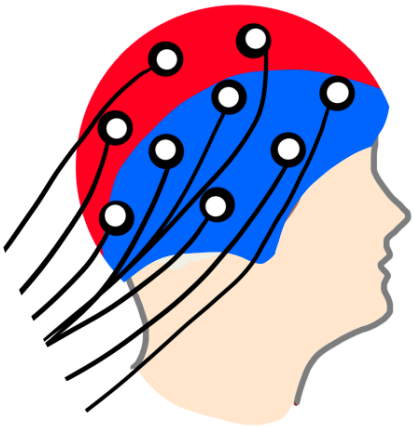

Figure 7 – EEG electrode placement

1.5. Current Source Estimation

Current source estimation is the methodology to solve the inverse ill-posed problem of localizing hundreds or thousands of vertices in the brain, and their associated currents, from the electric potential measured by a low number of MEG or EEG electrodes. The purpose of current source estimation methods is to increase the spatial resolution to millimetrical level.

There are two main types for current source estimation methods: dipole methods and distributed source methods. In the dipole method, approximating brain activity with the assumption that the neural activity of interest is confined to a small brain area solves the inverse problem of current source estimation (Silva, et al., 2004). The distributed source methods assume a large number of current dipoles distributed over the brain cortex to solve the inverse problem (Aihara, et al., 2011; Hämäläinen, et al., 1993). In the present research we estimate current sources over the sensorimotor areas in the brain, as well as sources distributed all over the brain cortex. For this reason, a distributed current source method was selected to find the solution for the inverse problem and to obtain current sources relevant to the experimental tasks of interest.

Some of the commonly known distributed source methods to estimate current sources from EEG, include the low resolution brain electromagnetic tomography (LORETA) (Pascual-Marqui, 1994, 2002, 2007) and the minimum norm estimates (Silva, et al., 2004) Methods that integrate fMRI as a prior, in order to increase the spatial resolution of estimated sources, include a variation of the dynamic statistical parametric mapping (dSPM) (Dale, et al., 2000), the Wiener filter or the Bayesian method (Dale, et al., 2000, Kajihara, et al., 2004; Phillips, et al, 2002; Schmidt, et al., 1999), and the hierarchical variational Bayesian estimation (VBMEG) (Sato, et al., 2004). Among these methods, VBMEG was selected in the current study for the following reasons: 1) VBMEG is a high-resolution method that can estimate thousands of current dipoles on the brain cortex and 2) current source estimation in VBMEG is less susceptible to incorrect prior information of the fMRI.

1.5.1. Cortical Current Source Estimation with VBMEG

Source estimation with the hierarchical variational Bayesian estimation (Sato, et al., 2004) was done in MATLAB with the VBMEG toolbox (VBMEG – Variational Bayesian Multimodal EncephaloGraphy, http://vbmeg.atr.jp/), using MRI, fMRI and EEG data. In the individual space, the MRI structural data provides a 3D model of the brain cortex, and the boundary information for white matter, gray matter and cerebrospinal fluid, to generate a three-shell model of the head (boundary element method). The fMRI provides information about a region of interest (where current dipoles are assumed), and the relative amplitude of the current in each vertex or dipole (Yoshioka, et al., 2008).

To estimate current sources in VBMEG, consider the relationship between the recorded EEG potentials in the scalp, and the current sources at time point t:

$$E(t) = G \cdot J(t)$$

Equation 1

Where $E(t)$ is the acquired EEG data, G is the leadfield matrix and $J(t)$ is the amplitude of the cortical current. Then, inverse problem consists in estimating $J(t)$ from the acquired EEG data $E(t)$.

The activity information derived from the fMRI, is imposed through hyperparameters as prior information on the current variance distribution, rather than the variance itself, with consideration of a spatial smoothness constraint. This constraint can be imposed as the structural constraint on the off-diagonal part of the covariance matrix, which enforces high correlations between neighboring current activities:

$$P_0(J_{1:T}|\alpha,\lambda) \propto exp\left[-\frac{1}{2}\sum_{t=1}^{T} J'(t) \cdot \sum\nolimits_{\alpha} \cdot J(t)\right]$$

Equation 2

Where the inverse variance parameter α, is estimated by introducing an Automatic Relevance Determination (ARD) [45] prior. α is considered a random parameter with Gamma distribution, and the fMRI information is imposed on the variance distribution, using two hyperparameters: a variance magnification parameter (μ_0) and a confidence parameter (γ_0). μ_0 controls the current amplitude for a given fMRI activation, and γ_0 controls the width of the prior distribution.

The current covariance matrix $\sum_{\alpha}^{-1}$ is represented by:

$$\sum_{\alpha}^{-1} = \mathrm{A}^{-1} + W \cdot \Lambda^{-1} \cdot W'$$

Equation 3

A and Λ are the diagonal matrices with diagonal elements $\alpha = \{\alpha_n | n = 1{:}N\}$ and $\lambda = \{\lambda_n | n = 1{:}N\}$, where α_n is the variance parameter controlling the the variance of the nth current, and λ_n is the smoothness parameter controlling the correlation between the nth and the neighboring currents. W is the Gaussian smoothing filter with a full width at half maximum of 6 mm, characterizing the spatial profile of the correlation function.

Finally, the inverse filter L is calculated using the estimated covariance matrix. After the inverse filter is estimated, current source estimation becomes a linear problem:

$$J(t) = L\left(\sum_{\alpha}^{-1}\right) \cdot E(t)$$

Equation 4

Further details about the variational Bayesian estimation method are found in (Sato, et al., 2004).

1.6. Classification

There are three main types of machine learning: unsupervised learning, reinforcement learning and supervised learning. In the unsupervised learning an agent learns without feedback; in the reinforcement learning the agent learns from rewards and punishments; and in the supervised learning, the agent learns from the observation of labeled data and estimates a function to map input to output (Russell and Norvig, 1995). The decoding of estimated current sources and preprocessed EEG sensor signals are a type of supervised learning, where the input features are the time-series belonging to a category (the experimental tasks).

Among supervised classifiers, support vector machines (SVM) (Boser, et al., 1992; Vapnik, 1999) and logistic regression are some of the commonly used methods for the decoding of time-series data. For the multi-class decoding of the brain data in this study, a variation of the logistic regression is used as a classifier; that is, a sparse logistic regression (SLR) method (Yamashita, et al., 2008) implemented in the SLR toolbox version 1.2.1 alpha (Advanced Telecommunications Research Institute International (ATR), Japan. http://www.cns.atr.jp/~oyamashi/SLR_WEB.html) for MATLAB.

SLR was selected over SVM for this study, because it performs better in the presence of irrelevant features, is less sensitive to overfitting, and does not require previous dimensionality reduction or manual parameter setup (Yamashita, et al., 2008).

1.6.1. Sparse Logistic Regression

SLR is an implementation of ARD to binary and multiclass classifiers based on logistic regression. For the purpose of multiclass decoding, each class has its own linear discriminant function, described by:

$$f_c(\boldsymbol{x}; \boldsymbol{\theta}^c) = \sum_{d=1}^{D} \theta_d^{(c)} x_d + \theta_0^{(c)}$$

Equation 5

Where $\boldsymbol{x} = (x_1, \dots x_D)^t$ is an input feature vector in D dimensional space, $\boldsymbol{\theta} = (\theta_1, \dots \theta_D)^t$ is a weight vector and c represents each class. The outputs of Equation 5 are transformed into the probability of observing each label (class) using the softmax function:

$$P(S_c|\boldsymbol{x}) = \frac{exp\left(f_c\left(\boldsymbol{x}: \boldsymbol{\theta}^{(c)}\right)\right)}{\sum_{k=1}^{c} exp\left(f_k(\boldsymbol{x}: \boldsymbol{\theta}^{(k)})\right)}$$

$$c = 1, 2, \dots C$$

Equation 6

The weight parameters are treated as random variables with prior distributions. A prior of each weight parameter is introduced as a relevance parameter, which controls the range of the corresponding weight parameter. Weight estimation is an iterative algorithm that updates weight parameters while updating relevance parameters, and updating relevance parameters while fixing weight parameters. The associated weights of the relevance parameters that diverge to infinity becomes zeroes, therefore the associated features are pruned form the model. Further details of ARD applied to the MLR can be found in (Yamashita, et al., 2008).

1.7. Objectives of the Study

The purpose of the study is to design a decoder for walking related tasks, based on non-invasive brain signal recordings, that can provide an insight of an online BCI to control an exoskeleton or a functional electrical stimulation system.

In this study, non-invasive brain signal recordings as EEG, fMRI and MRI are acquired from healthy participants during the execution of ankle flexion and extension at two force levels, considering that these tasks have an important contribution to the normal walking cycle in humans. EEG, fMRI and MRI are used to estimate cortical current sources applying a hierarchical variational Bayesian estimation (VBMEG) for each of the experimental tasks. Finally, the time-series of preprocessed EEG sensor signals and the estimated current sources are decoded with a multi-class sparse logistic regression classifier (SLR).

Among the distributed current source estimation methods that can also integrate fMRI as prior information, VBMEG was selected because the method has shown a better performance than conventional linear inverse filter methods, and less degradation of current estimates when incorrect fMRI information is given (Yoshioika, et al., 2008). On the other hand, SLR was selected mainly because it is more robust in the presence of irrelevant features, when compared to other methods such as support vector machine (SVM) and regularized logistic regression (RLR) (Yamashita, et al., 2008).

Current decoders based on EEG can perform binary classifications to detect the intention of movement (movement vs. still). Another approaches are aimed to detect the movement intention of each leg (Hashimoto, et al., 2013), reaching and grasping tasks (Schwarz, et al., 2018), or perform multi-class classifications of hand movement directions (Robinson, et al., 2013). We aim to perform 9-multiclass classification of leg movements, which is a challenge considering the low spatial resolution of the EEG and that the anatomical areas in the brain related to legs and feet movements are located in the central portion of the frontal lobe, in comparison with the brain areas related to arms movement which are located towards the laterals of the frontal lobe. To overcome these limitations, a combination of VBMEG and SLR is applied in this study, since it has shown good performance in previous studies (Morioka, et al., 2013; Yoshimura, et al., 2016). In this regard, this research is aimed to design a brain-signal decoder for walking that can detect multiple motor tasks instead of only movement intention.

Chapter 2: Experimental and Preprocessing Methods

This chapter introduces the experimental design and the preprocessing techniques used in the study: the conducted experiments and the motor tasks of interest are described, followed by the specification of the experimental paradigms and the preprocessing techniques applied to the acquired data. The preprocessed data obtained from the techniques described in this chapter, are used as inputs in the analyses in Chapters 3 and 4.

2.1. Experimental Design

Two types of experiments were conducted for this research on different days: an EEG experiment and an fMRI experiment. The experiments were performed on 8 healthy participants (5 males and 3 females) aged 22–50 years (Mean: 29.67 ± 8.81). In both EEG and fMRI experimental paradigms the same cue images were used.

In line with the objective of this study of decoding walking-related tasks, the experiments were based on 8 isometric ankle flexion (dorsiflexion) and extension (plantarflexion) tasks at high and low force levels, and 1 control (still) task, because these are an important part of the normal gait cycle in humans. The experimental tasks and images are shown in Figure 8. To achieve the isometric contraction in both experiments and reduce movement artifacts inside the MRI scanner, a custom-made platform (Right Mfg. Co., Ltd, Tokyo, Japan) with detachable Velcro stripes was used to fix the feet of the participants, as shown in Figure 9 and 10. Additionally, electromyographic (EMG) activity was measured in both EEG and fMRI experiments, with the sole purpose to confirm task execution and this data was not included in the decoding analyses.

Other walking-related tasks such as knee flexion and extension were not included in the experimental paradigm, because performing these motor tasks can cause a large error in the acquisition of fMRI data, induced by the movement of the head inside the MRI scanner. During a typical fMRI scanning session of the brain, the head of the participant is fixed with cushions, to reduce head movements (ideally to limit the head movement within 3 mm in each direction), and keep the participant comfortable throughout the experimental session.

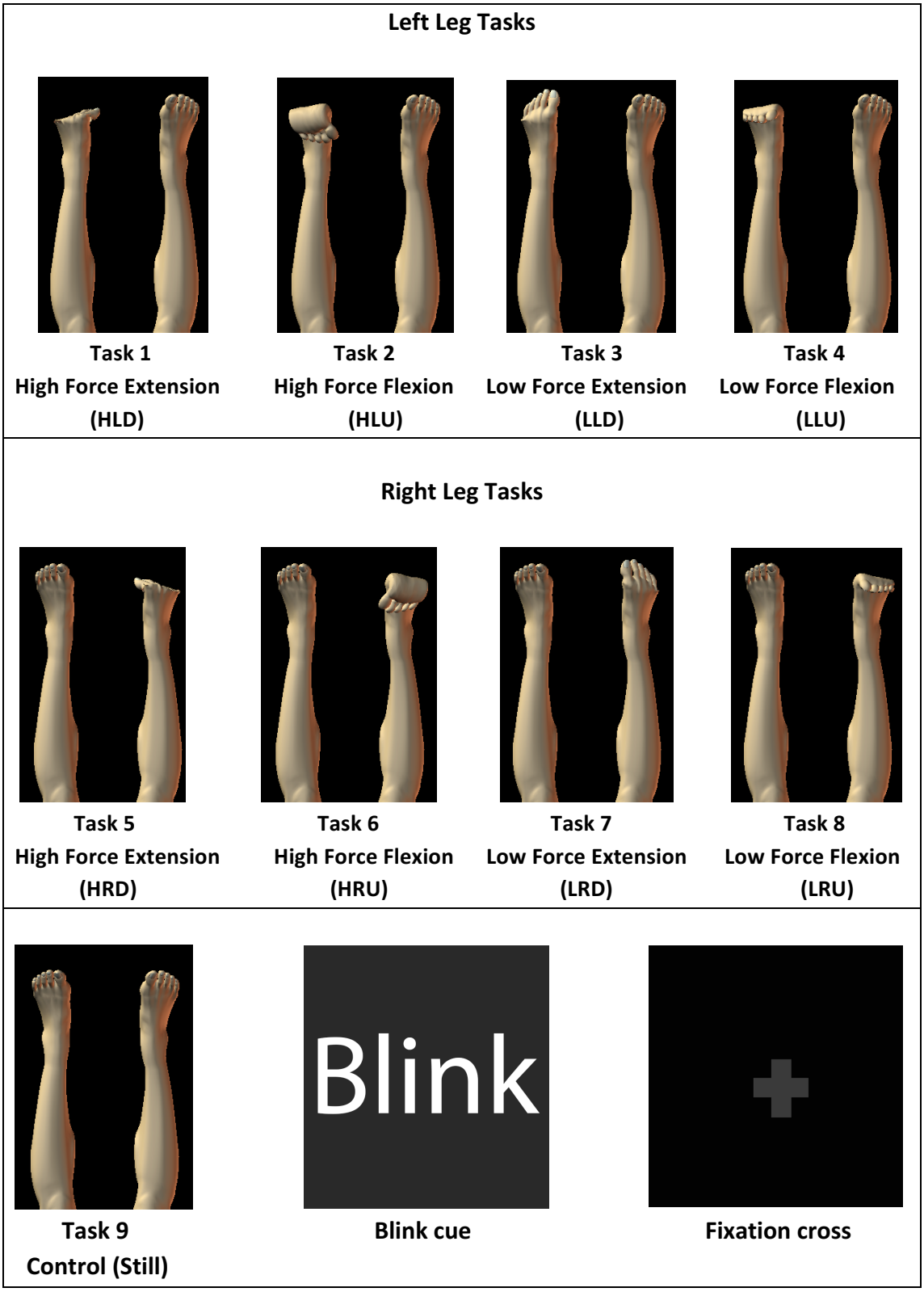

Figure 8 - Experimental tasks and images used for the fMRI and EEG experiments. The cross fixation and the blink cue were used only during the EEG experiment.

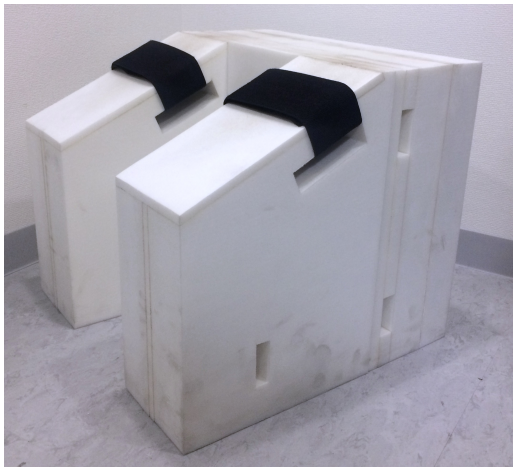

Figure 9 – Custom-made platform to fix the participant's feet during the EEG experiment.

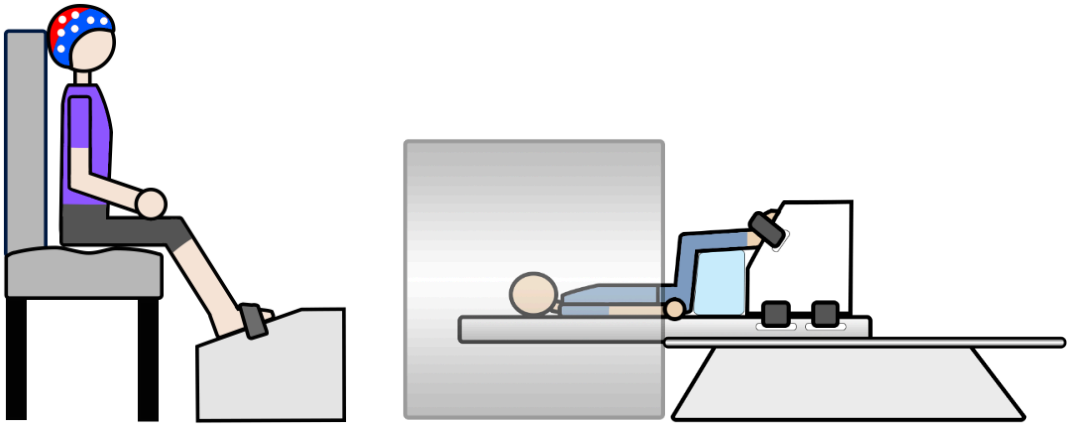

Figure 10 – Positioning of the participant during the EEG experiment (left) and the fMRI experiment (right).

MRI/fMRI Experimental Paradigm

The fMRI experimental paradigm was created in Presentation 16.3 (Neurobehavioral Systems, Inc., California, United States), and consisted of one session with 7 runs. Each run included 9 task execution blocks (8 active tasks and 1 control task). Inside each block, a randomly selected experimental task was executed for 2 s followed by 1 s of rest. This set of task execution and rest was repeated 6 times, resulting in duration of 18 s per block. Figure 11 illustrates the fMRI experimental session.

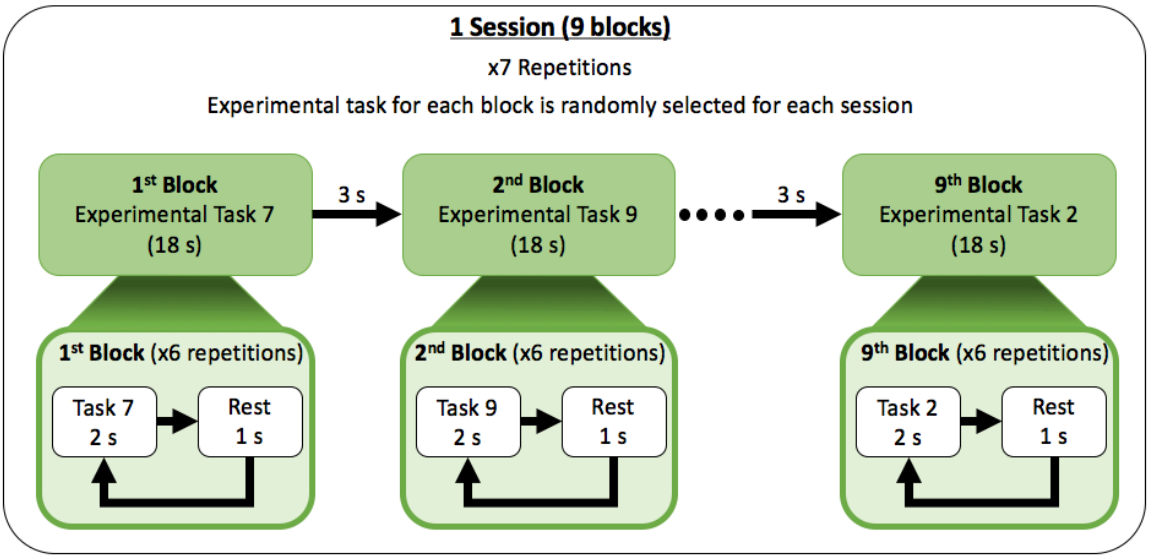

Figure 11 – Experimental session for the fMRI experiment

EEG Experimental Paradigm

The EEG experimental paradigm was created in MATLAB 2013b (The MathWorks, Inc., United States), and consisted of one session with 3 modules as follows: "Module 1 – Flexion and Extension", "Module 2 – Right and Left" and "Module 3 – High Force and Low Force". Inside each module, one set composed by two active experimental tasks and the control task, was repeated 5 times. In each set, each task was repeated 2 times and the control task was repeated once therefore, at the end of each set execution, 10 trials of each active task and 5 trials of the control task were acquired. Each set was repeated 2 times before changing the active experimental tasks. Figure 12 illustrates the EEG experimental session.

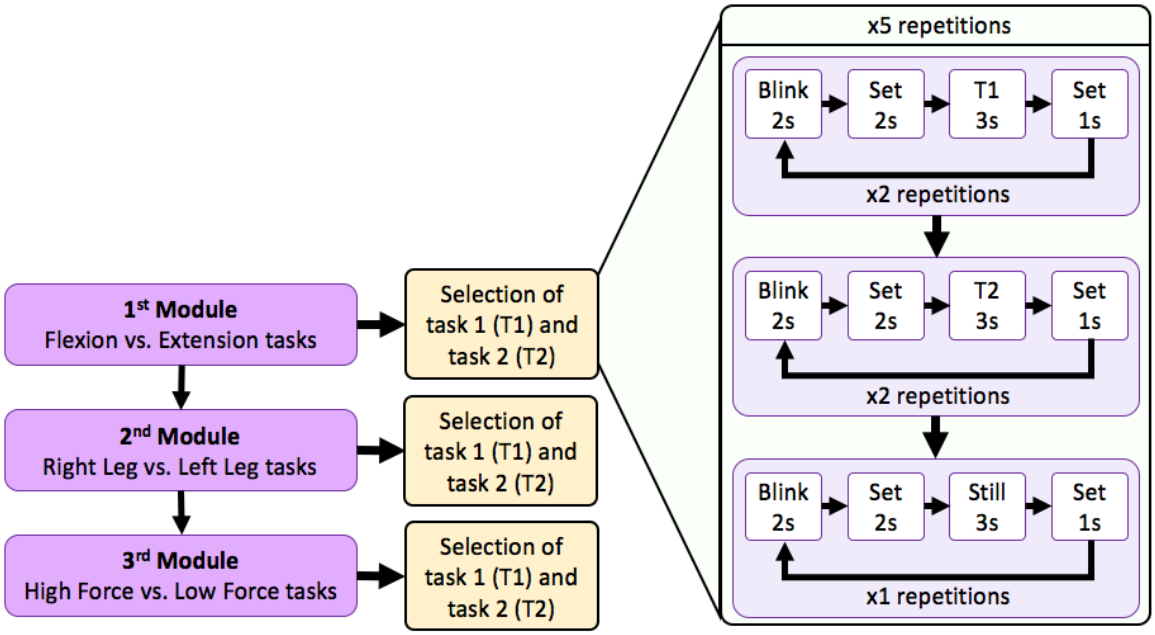

Figure 12 – Experimental session for the EEG experiment

2.2. Ethics Statement

The ethics committee of Tokyo Institute of Technology and the ethics committee from the National Center of Neurology and Psychiatry (NCNP) approved the informed consents used in this study.

At the beginning of the experimental sessions, each participant was informed about the procedures carried out during the experiments, asked in a questionnaire about possible exclusion criteria from the study and explain their right to freely stop the experiment at any stage.

2.3. MRI and fMRI Experiments

The MRI and fMRI experiments were carried out in the National Center of Neurology and Psychiatry using a 3 Tesla Verio MRI Scanner (Siemens AG, Munich, Germany). Three types of images were acquired: two T1-weighted structural including sagittal and axial scans (MRI), and T2*-weighted functional images (fMRI). The MRI images were obtained with a magnetization prepared rapid gradient-echo (MPRAGE), and the fMRI images were obtained with echo planar imaging (EPI) using a generalized autocalibrating partial parallel acquisition (GRAPPA) method. It is worth mentioning that from now, the words EPI and fMRI will be used indistinctively throughout this manuscript to refer to the functional images. The parameters used to acquire the images are shown in Table 1.

Parameter	**MRI**		**fMRI**
Orientation	Sagittal	Axial	
Number of slices	224	48	116 volumes per session
Voxel size	1 x 1 x 1 mm	1 x 1 x 1 mm	3 x 3 x 3 mm
Repetition time (TR)	2 s	2 s	2 s
Echo time (TE)	3.4 ms	3.4 ms	13 ms
Flip angle	8°	8°	90°
Field of view (FOV)	256 x 256 mm	192 x 192 mm	192 x 192 mm
Imaging matrix	256 x 256	192 x 192	64 x 64
Inversion time	0.99 ms	0.99 ms	-

Table 1 – MRI and fMRI recording parameters

EMG signals from ankle flexors and extensors (Tibialis Anterior: dorsiflexor; Gastrocnemius: plantarflexor and knee flexor; Soleus: plantarflexor; Extensor Hallucis Brevis: toes extensor) was recorded using 8 pairs of Ag/AgCl electrodes with a BrainAmp ExG MR system (Brain Products GmbH, Gilching, Germany).

2.4. EEG Experiment

EEG data was acquired with an ActiveTwo BIOSEMI system (BIOSEMI, Amsterdam, Netherlands), using 32 Ag/AgCl active electrodes placed accordingly to the 10–20 international system layout, and two reference electrodes placed on the right and left earlobes. In preparation for placing the electrodes, the cap gaps were filled with highly conductive gel and the earlobes were cleaned with 70% ethanol. EEG signals were recorded using the ActiView software with a sampling rate of 256 Hz, and the position of the electrodes was recorded with a Polaris Spectra (Northern Digital Inc., Waterloo, Canada). EMG data was recorded with 8 single differential electrodes using a Bagnoli™ Desktop EMG System (Delsys, United States). This experiment was conducted in a soundproof room (AMC-3515, O'HARA & Co., Ltd.) with a 24” monitor showing the experiment directions.

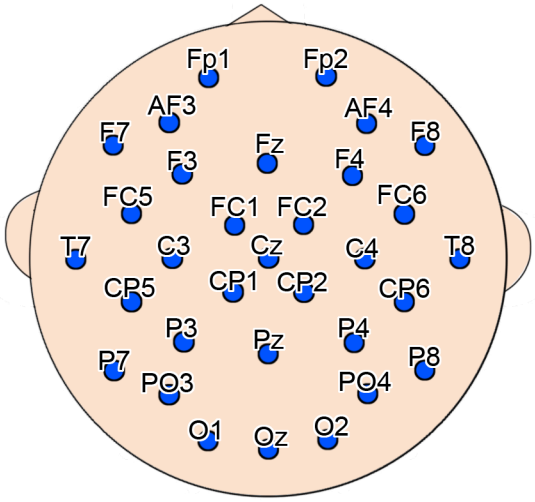

Figure 13 – Distribution of 32 EEG electrodes according to the extended 10-20 system

2.5. Data Preprocessing

MRI and fMRI recordings were preprocessed to obtain brain models for each participant, and to extract area and activity information to be used as priors for the current source estimation in VBMEG. From the MRI, a 3D polygon model of the brain cortex containing single-current dipoles equidistantly distributed and perpendicular to the cortex, were obtained for each participant along with the corresponding three-shell model of cerebrospinal fluid, skull and scalp. From the fMRI area and activity priors were obtained. The area prior was obtained as the coordinate values of statistically significant voxels, and the activity prior as the t-values corresponding to the vertices of the area prior. These priors were used to estimate EEG current sources on the brain cortex.

2.5.1. MRI and fMRI Data Preprocessing

MRI and fMRI data was recorded in DICOM format and converted into ANALYZE 7.5 format using the conversion tool included in the VBMEG toolbox. The ANALYZE 7.5 format is

composed of two files: one image file (.img) that contains the voxel intensities, and a header file (.hdr) containing the technical specifications of the image file.

To preprocess the MRI and fMRI data, the SPM8 toolbox (Wellcome Department of Cognitive Neurology, UK; http://www.fil.ion.ucl.ac.uk/spm) for MATLAB was used. Two types of analyses were performed: an individual analysis and a group analysis. Figure 14 shows the flow of the MRI/fMRI preprocessing in SPM8.

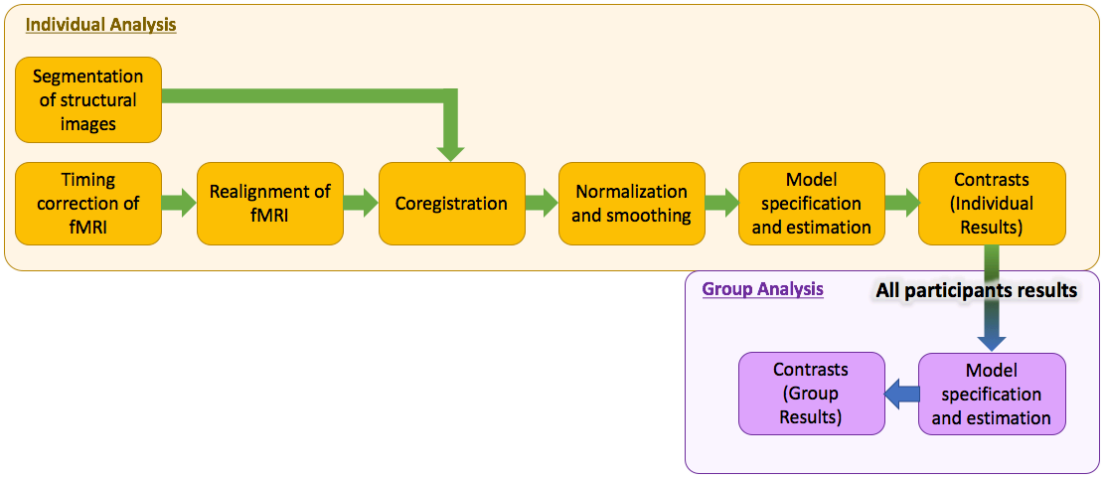

Figure 14 – Preprocessing pipeline in SPM8 to obtain contrasts for a group analysis.

Individual Analysis (1st Level)

The first images to process are the structural MRI sagittal and axial scans. These images were bias corrected and segmented into gray and white matter, using a probabilistic atlas of the brain. For the preprocessing of the functional images, the first five volumes of the EPIs, when the magnetization is still not stable, were discarded. The remaining EPIs were corrected for differences in acquisition time: this process aligns all the slice data to the same point in time. Then, the corrected EPIs were spatially realigned to the mean of all EPIs, with the purpose of removing movement artifacts. After segmentation, and temporal and spatial alignments pre-processing, the EPIs were ready to be interpolated (mapped) to the high-resolution structural sagittal image in the coregistration step. The next step was to normalize the coregistered images, to a template with the standard brain coordinates from the Montreal Neurological Institute (MNI), and smoothed with a full-width spatial Gaussian kernel of 8 mm at half maximum. At this step the fMRI and MRI preprocessing is done, and what followed next was the model specification and estimation using the general linear model (GLM), defined as:

$$Y = X\beta + \varepsilon$$

Equation 7

Where Y is the recorded time course of each voxel (the preprocessed fMRI data), X is the design matrix containing the convolution of boxcar functions (the onsets and durations of the 9 experimental tasks) with the canonical hemodynamic response (hrf), β is the calculated weight to X that quantifies the potential contribution of predictor X in explaining the voxel time course Y, and ε is the error between the observed data and the predicted data. Having estimated the model parameters, the final step in the individual analysis was defining the contrast vectors to produce statistical parametric maps for each experimental task. For the 9 experimental tasks used in this experiment, consider Task 1 as high force extension in the left leg (HLE), and Task 2 as high force flexion in the left leg (HLF), therefore a contrast vector to pick out any voxels related to Task 1 will be [1 0 0 0 0 0 0 0 0], and for Task 2 [0 1 0 0 0 0 0 0 0], and so on. These analyses were applied to obtain parametric maps of each participant, and the results obtained from all participants were then used together as inputs for the group analysis.

Group Analysis (2nd Level)

A group analysis was performed using a full factorial design to obtain statistical parametric maps common for all the participants. The design specification consisted of three factors with two levels each, as follows: Factor 1: Left Leg and Right Leg, Factor 2: Flexion and Extension and Factor 3: High Force and Low Force. After parameter estimation, T-contrasts to obtain statistical parametric maps related to all the left leg tasks (4 tasks: high force flexion, high force extension, low force flexion and low force extension) and the right leg tasks (4 tasks: high force flexion, high force extension, low force flexion and low force extension) were obtained with a threshold of $p < 0.01$ (uncorrected for multiple comparisons).

The final objective of the fMRI analysis was to obtain the area (region of interest) and activity (voxel intensities) that contribute mostly to the experimental motor tasks in the ankle. To obtain this information, a mask including Brodmann areas 1,2 and 3 (primary somatosensory cortex), Brodmann area 4 (primary motor cortex), and Brodmann area 6 (premotor cortex and supplementary motor area) was applied to the group analysis results. These Brodmann areas were included since they are well known to contribute to motor planning and execution. The mask was created using the WFU PickAtlas (Radiology Informatics and Imaging Laboratory, USA; http://fmri.wfubmc.edu/software/pickatlas) tool for SPM. The masked results from the group analysis were inversely normalized to individual participant's space using the VBMEG function “vb_job_convert_spm.m”. After this, the results were ready to be used for current source estimation in the VBMEG toolbox.

All the default SPM8 parameters for preprocessing have been used in this preprocessing. For the reader interested in learning more about the details and functions used in preprocessing step, please refer to the documentation of each function in the SPM8 toolbox.

2.5.2. EEG Data Preprocessing

EEG data was preprocessed with two different approaches for the analyses described in Chapter 3: Classification of Motor Tasks in the Ankle, and Chapter 4: Effect of the Reducing Number of EEG Electrodes on the Classification Accuracy. For the first analysis performed (Chapter 3), the EEG data was filtered and epoched, while for the second analysis (Chapter 4) the data was further inspected for artifacts using independent component analysis (ICA).

EEG Acquisition

The EEG data was recorded in BDF format using a BIOSEMI acquisition system (BIOSEMI, Amsterdam, Netherlands) at 256Hz, and converted into MATLAB format using the EEGLab Toolbox EEGlab (Delorme and Makeig, 2004, https://sccn.ucsd.edu/wiki/EEGLAB). From this point forward, the imported EEG data went through two preprocessing flows in order to obtain the datasets used as inputs for the analyses performed in Chapter 3 and Chapter 4.

EEG Preprocessing for Chapter 3

The imported EEG data was band-pass filtered between 0.5 and 40Hz, downsampled to 200Hz, and epoched in segments of -0.5 s pre-onset (in reference to the experimental image presentation cue), to 3 s after onset. As a result, 50 trials for each of the 9 experimental tasks were obtained for each participant. This preprocessed EEG signals were used as an input to the SLR classifier, and as inputs for the current source estimation in VBMEG.

EEG Preprocessing for Chapter 4

One of the objectives of the analysis in Chapter 4, is to take a step closer into the development of a real-time BCI. Under controlled experimental conditions, blinking and movements can be restricted to some extent, however in a future BCI development the interface should include a module to remove artifacts caused by eye movements, blinking, muscle contraction, etc., to be able to achieve a good classification performance in daily life conditions. For this reason, the preparation of the EEG data for Chapter 4 included ICA to remove artifacts that could remain after filtering.

The imported EEG data was band-pass filtered from 2 to 39 Hz, resampled to 200 Hz, and epoched in segments of -0.5 s pre-onset (in reference to the experimental image presentation cue), to 3 s after onset for each task. As a result, 50 trials for each of the 9 experimental tasks were obtained for each participant.

To prepare for artifact removal, we appended in one single 32 EEG channel dataset, all trials and tasks for each participant, obtaining a dataset of 450 trials (50 trials x 9 tasks). From this dataset containing all 32 EEG channels, subdatasets of 16 and 8 channels configurations were

extracted, as shown in Figure 15. The 32 channels configuration corresponds to the extended 10-20 international system. The configuration for 16 electrodes, and the two configurations for 8 electrodes were decided based on their distribution over the sensorimotor areas.

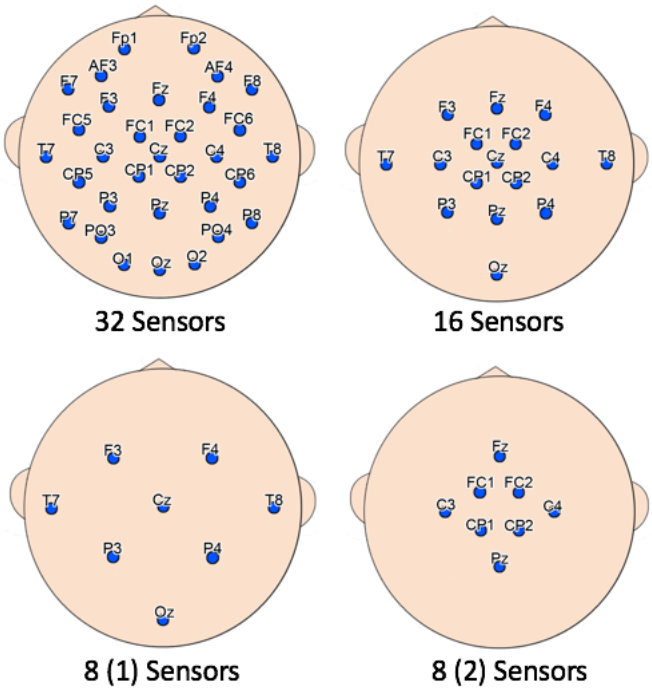

Figure 15 – Distribution of EEG electrodes for one configuration of 32 channels, one configuration of 16 channels and two configurations of 8 channels.

Independent component analysis (ICA) using EEGLab, was applied to each of the 32, 16 and 8(1) and 8(2) channels datasets of each participant. The selection of ICs to be pruned was done by visual inspection of topographic patterns and power graphs, and partially assisted by the MARA plugin (https://irenne.github.io/artifacts/). An example of ICs for an 8-channel configuration is shown in Figure 15. The cleaned datasets were than used as inputs for the classification of EEG signals, and to estimate current sources.

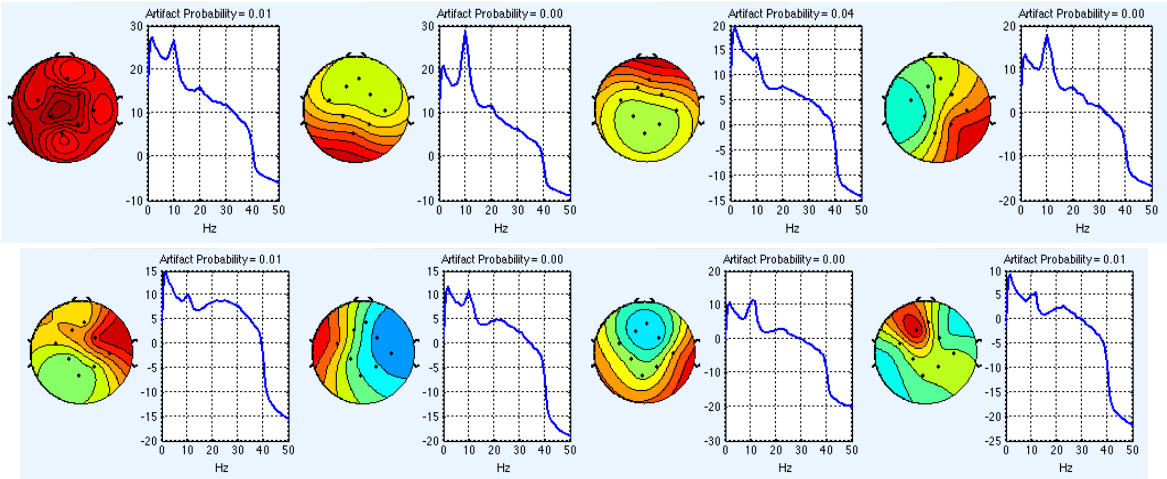

Figure 16 – An example of ICs obtained for the 8(2) channel configuration, in a representative participant.

2.5.3. Brain Modeling

After the preprocessing of MRI, fMRI and EEG data, the estimation of cortical current sources in VBMEG follows. This estimation can be broadly divided into two steps: 1) brain modeling and 2) current variance and current time course estimations. The brain modeling will be described in the following paragraphs, while the current variance and current time course estimations will be included in Chapter 3 and Chapter 4, as these parameters are different for each analysis. All the VBMEG analysis were done according to the standard procedures described in the documentation available in http://vbmeg.atr.jp/docs/v2/static/vbmeg_users_manual.html.

Brain models were obtained for each participant as polygon models composed by 10,004 ~ 20,004 single-current dipoles equidistantly distributed on and perpendicular to the cortical surface. These models were obtained from the segmented and bias-corrected image from the sagittal MRI, using FreeSurfer (Martinos Center Software, https://surfer.nmr.mgh.harvard.edu/). Information about the boundary information of the scalp, the skull and the cerebrospinal fluid (CSF) was also obtained from FreeSurfer. This information is imported into VBMEG to extract the cortical model of the brain and a three-shell model of the head as shown in Figure 17.

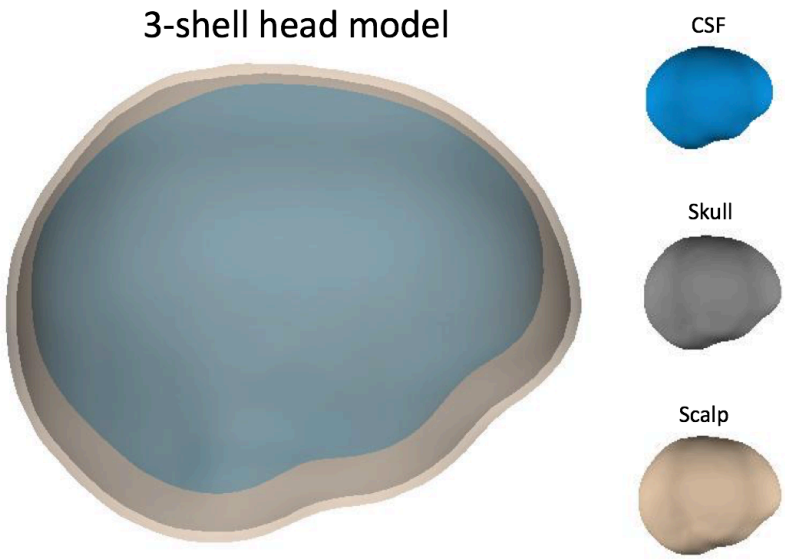

Figure 17 – 3-shell model of the brain, containing the cerebrospinal fluid (CSF), the skull and the scalp.

In the final step of the brain modeling, the leadfield matrix is calculated using a boundary elementary method (three-shell BEM: a geometrical model describing the interaction among skull, scalp and brain), the cortical surface model and the EEG sensor positions.

Chapter 3: Classification of Motor Tasks in the Ankle

The objective of this chapter is to investigate whether estimated current dipoles located in brain areas well known for contributing to movement planning and execution, are sufficient to design a decoder capable of classifying 9 tasks (8 active motor tasks and 1 control task) from non-invasive brain signal recordings.

The preprocessed fMRI and EEG data, and the brain model (Chapter 2.5. Data Preprocessing) are used as inputs for the analysis described in this chapter. Firstly, the parameters for current source estimation and classification are described, and secondly the results are shown along with the discussion.

3.1. Current Source Estimation Parameters

Parametric maps obtained from the fMRI group analysis in Chapter 2.5.1, were inversely normalized into participant' space using the "vb_job_convert.m" function included in the VBMEG toolbox. As a result, two types of prior information were obtained: an area prior and an activity prior as shown in Figure 18.

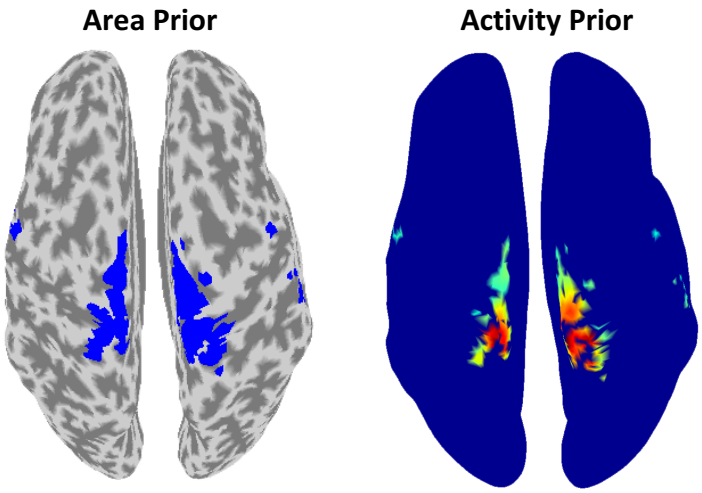

Figure 18 – Area and activity priors mapped on a representative participant's brain. These priors are obtained from the fMRI group analysis, and inversely normalized to each participant's space.

Time-series of cortical current sources are estimated from the preprocessed EEG data using the brain models obtained in Chapter 2.5.3. To estimate the current variance, the period from -0.5 to 0 s of each EEG trial was used as a baseline, and the area and activity priors were imposed on the prior distribution of the current variance with the hyperparameters $\mu 0 = 10$

and γ0 = 1, because the fMRI and EEG experiments were conducted on different days (contrarily, high values for both μ0 and γ0 indicated the brain activity was the same for both experiments). For the inverse filter estimation, the EEG data (-0.5 s to 3 s) was divided into 14 windows of 0.5 s of length each, overlapping for 0.25 s. Dipole reduction ratios were set individually for each participant to reduce the number of vertices from 20,004 to around 200. With these parameters the inverse filter is estimated for each of the 14 windows. After the inverse filter estimation, current source estimation becomes a linear problem and current sources time-series are estimated from the EEG data as in equation 4.

Labeling of current sources vertices

The brain model includes the MNI coordinates of the dipoles. Since the normalization process from individual space MRI/fMRI is not perfect, it is common (and expected) to find some vertices outside (or overlapping) the original region of interest. The vertices were labelled using the probabilistic cytoarchitectonic maps included in the Anatomy toolbox v1.8 (Institute of Neuroscience and Medicine (INM-1), Germany) for SPM8. Upon inspection of the vertices labels, we discarded the current sources that might not belong (or may not have a strong relationship) with the brain activations of interest, and/or to the experimental paradigm itself.

3.2. Classification of EEG and Estimated Cortical Current Sources

The estimated current sources time-series and the preprocessed EEG data time-series, were used as inputs for the multi-class SLR classifiers. Each of the 9 experimental task consisted of 50 trials of 3.5 s each. These epochs of data were downsampled to 30 Hz, and the epoch from 0 s to 1.5 s was used as inputs for the classifiers. The 9-class classifications were done using a leave-one-out method (LOO). The classification for current sources was conducted separately from the EEG, therefore each classifier was decoding 9 experimental tasks for EEG, and 9 experimental tasks for current sources. Among the classification functions from the SLR Toolbox, the SLR-VAR (SLR with variational approximation) function was used, because it was the fastest and it had the less memory use according to the SLR toolbox documentation.

As a result, the mean classification accuracy for the 9 classes was obtained, along with confusion tables and weight matrices showing the features that contributed the most to the classification accuracy. Additionally, 5-classes classifications were performed for the tasks executed in each leg (4-active right leg tasks and the control task, and 4-active left leg tasks and the control task). The results of this chapter are shown in the next section, 3.3 Results. Significance values were obtained from permutation tests and corrected for multiple comparisons using a false discovery rate (FDR) of 0.05 (Nichols and Homes, 2003).

3.3. Results and Discussion

The number of dipoles located over the brain cortex model of each participant is of 20,004 dipoles. The number of dipoles was reduced down to 188 in average, due to the area prior introduced by the fMRI and the use of a dipole reduction ratio, set up individually for each participant.

Participant	1	2	3	4	5	6	7	8
# of Current Sources	194	188	174	193	181	194	190	190
Mean	188 ± 7.07							

Table 2 – Number of current source estimated for each participant

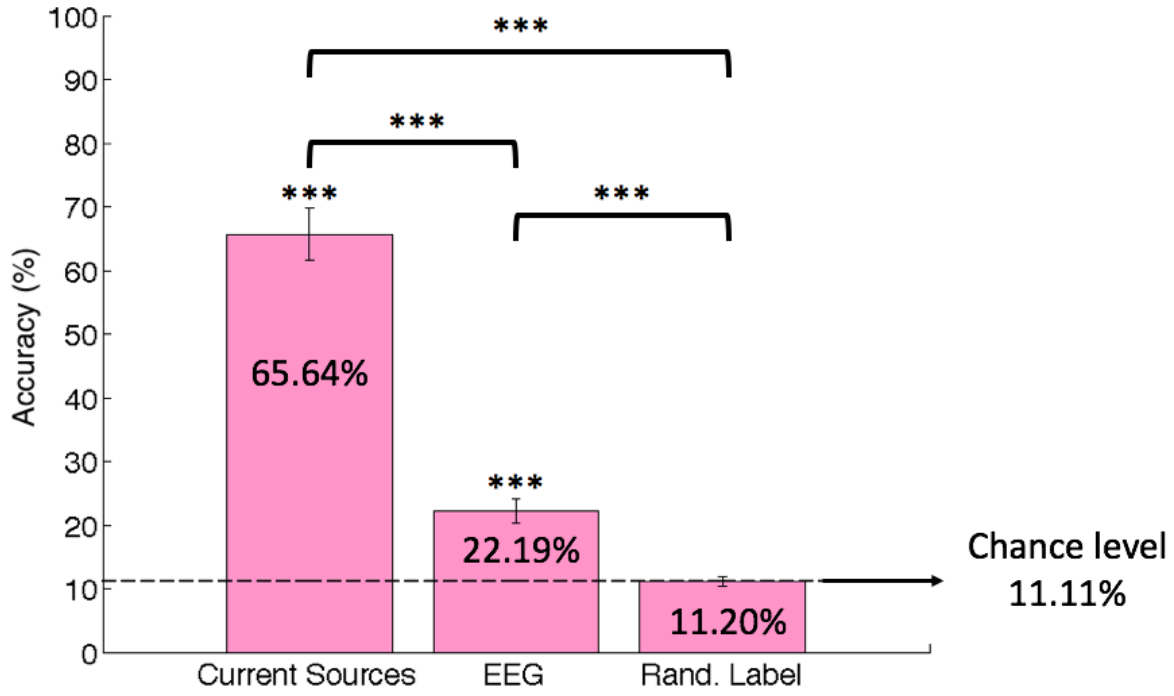

Figure 19 – Classification accuracies obtained for the 9-class decoding of estimated current sources, preprocessed EEG sensor signals and the average of the randomized label for current sources and EEG across participants.

Figure 19 shows the mean classification accuracies for the classification of current sources, EEG and randomized label. The mean accuracy for current sources classification was significantly higher than chance level (Current sources: 65.64% ±4.11; p = 1.19e−04), and than EEG sensor signals (EEG: 22.19%; p = 1.19e-04). The randomized level accuracy showed a non-significant value close to chance level, indicating that the high classification accuracy of the current sources was not due to an increase in dimensionality.

Target \ Selected	HLD	HLU	HRD	HRU	LLD	LLU	LRD	LRU	Still
HLD	31.63	2.63	2.25	1.25	2.25	2.63	2.00	1.63	3.75
HLU	1.00	35.50	1.25	1.88	2.50	3.25	1.38	1.00	2.25
HRD	2.38	1.38	35.38	1.38	1.38	2.00	3.25	1.00	1.88
HRU	1.00	2.25	1.63	34.63	1.00	2.38	1.88	3.13	2.13
LLD	1.50	2.75	2.00	1.38	32.75	2.75	2.13	1.88	2.88
LLU	1.88	3.38	1.25	2.38	3.25	29.75	2.13	2.00	4.00
LRD	1.25	1.75	2.13	2.63	2.63	3.13	29.75	2.38	4.38
LRU	2.00	1.50	1.00	2.25	1.13	3.38	2.13	34.25	2.38
Still	1.88	1.38	1.25	1.25	3.25	4.38	2.75	2.13	31.75
Class Accuracy (%)	63.25 ± 8.28	71 ± 8.90	70.75 ± 6.26	69.25 ± 6.80	65.5 ± 8.40	59.5 ± 11.99	59.5 ± 6.58	68.5 ± 6.59	63.5 ± 7.11
Average Accuracy (%)	65.64 ± 4.11								

Table 3 – Averaged confusion table across trials and participants, for the classification of current sources

Target \ Selected	HLD	HLU	HRD	HRU	LLD	LLU	LRD	LRU	Still
HLD	9.00	6.50	5.75	4.75	6.00	6.38	4.13	3.88	3.63
HLU	7.13	9.13	4.13	4.88	5.75	7.25	3.13	3.38	5.25
HRD	4.00	4.25	10.75	8.25	3.38	3.75	6.63	6.00	3.00
HRU	4.88	4.88	6.75	11.13	3.25	3.25	4.75	6.75	4.38
LLD	5.88	6.00	4.38	3.00	10.63	7.50	5.13	3.25	4.25
LLU	7.13	6.25	4.50	2.50	6.00	9.50	4.38	3.88	5.88
LRD	5.25	3.50	6.50	5.38	4.63	3.88	10.63	6.25	4.00
LRU	4.00	3.00	4.75	7.75	3.63	3.88	6.38	12.63	4.00
Still	3.13	5.25	2.25	3.50	4.38	5.38	4.38	5.25	16.50
Class Accuracy (%)	18 ± 3.25	18.25 ± 2.70	21.5 ± 2.76	22.25 ± 3.64	21.25 ± 3.81	19 ± 2.45	21.25 ± 3.85	25.25 ± 4.41	33 ± 8.52
Average Accuracy (%)	22.19 ± 1.85								

Table 4 – Averaged confusion table across trials and participants, for the classification of preprocessed EEG sensor signals

We attribute the high classification accuracy to the combination of current source estimation by VBMEG and classification by SLR, because redundant (but not identical) current source time-series are estimated for each task, and this provides the classifier with many candidates for feature selection. Furthermore, a study by (Yoshimura, et al., 2012) succeeded in reconstructing muscle activity from current sources estimated from 32 EEG channels using VBMEG and a sparse regression method, supporting further the high performance of the VBMEG method.

Aiming to a general approach, all the vertices from both left and right brain hemispheres obtained from a group analysis were used for the 9-classes classification results shown in Figure 19, however classifications for each leg were also performed using only the vertices located in the contralateral brain using parametric maps obtained for each participant (Chapter 2.5.1. MRI and fMRI Data Preprocessing - Individual Analysis (1st Level)): vertices in the right brain were used to decode the movements of the left leg, and vertices in the left brain were used to decode the movements of the right leg.

Figure 20 shows the mean classification accuracies for the classification of current sources, EEG and randomized label for the tasks in each leg. The mean accuracy for current sources

classification was significantly higher than chance level (20% for 5-classes) and EEG sensor signals, for the right leg (current sources: 73.55% ±2.83; p = 3.60e-04, EEG: 32.10% ±3.07; p = 3.60e-04) and the left leg (current sources: 70.55% ±5.31; p = 2.40e-04, EEG: 31.40% ±2.69; p = 2.40e-04) classifications. The randomized level accuracy showed a non-significant value close to chance level, indicating that the high classification accuracy of the current sources was not due to an increase in dimensionality.

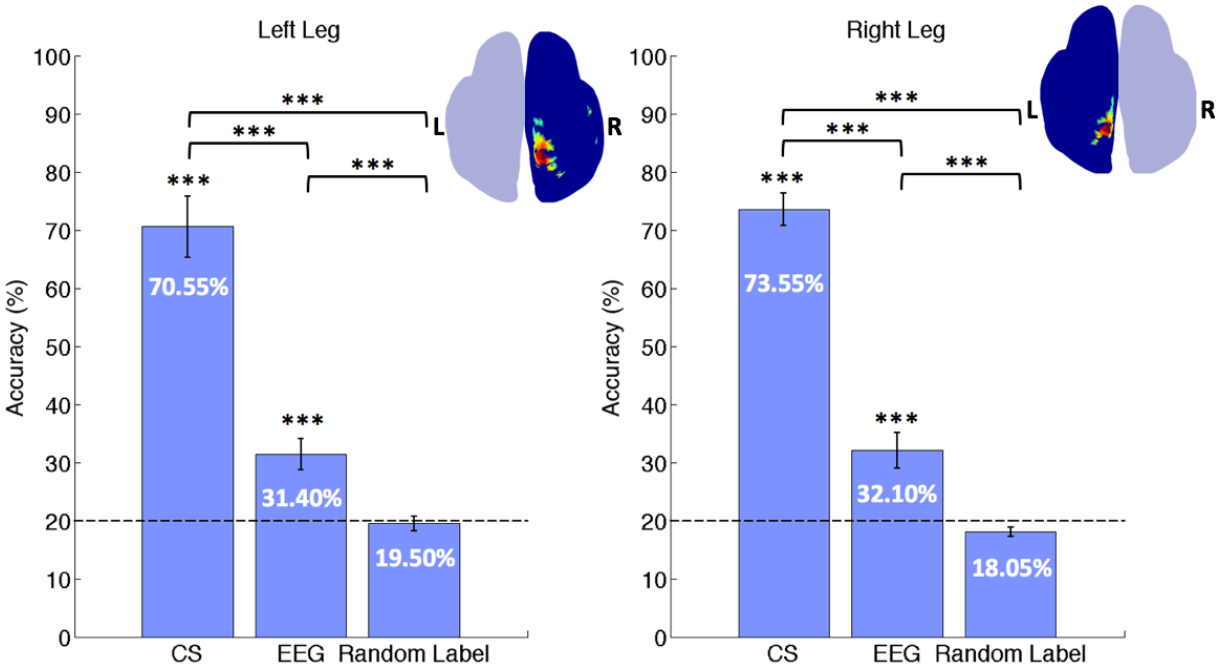

Figure 20 – Classification accuracies obtained for each of the 5-class decoding (left leg and right leg) of estimated current sources, preprocessed EEG sensor signals and the average of the randomized label across participants.

High accuracies were obtained for current sources even though the region of interest was small (limited to the areas in the brain related to feet movement). This result could be related to the high quality in the current source estimation of VBMEG when using prior information obtained from the high resolution fMRI information: A study by (Aihara et al., 2012) evaluated simulated and real EEG data under priors of different resolutions, and it was found that the use of 19 EEG channels along with the lowest resolution priors, outperformed the use of 64 EEG channels without any prior information. Even though it is impossible to determine the true origin of the current source, it is also considered that performing the same experimental tasks during both the fMRI and the EEG experiments could have increased the localization accuracy of current sources relevant to each task.

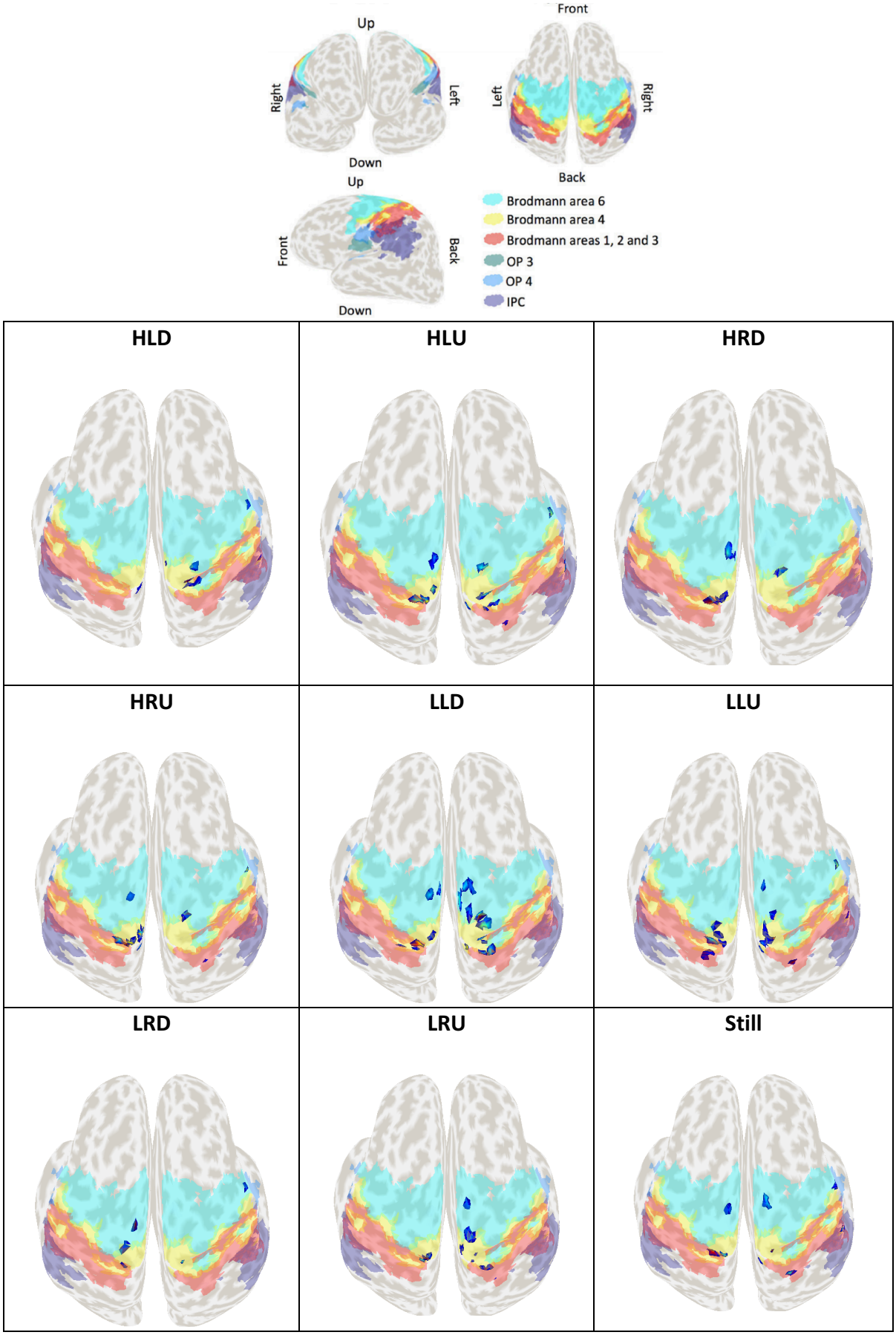

Figure 21– Selected current sources vertices by the SLR classifier, on a representative participant.

A weight analysis was also performed to obtain the current sources that contributed the most to each experimental task in each participant. The weights obtained from the SLR classification, were averaged and normalized across time-points and trials, and plotted on the cortical model. Figure 21 shows the selected current sources in the 9-class decoding, for a representative participant, plotted on the brain model.

Different activation patterns were obtained for each task and participant. Across tasks, the same number of vertices (in each participant) was used; therefore it was common to find the same vertex selected by the classifier for two or more tasks. However, the current time-series of the same vertex is different for each task, as well as the weight assigned by the classifier, therefore same vertices could be used for different classification of tasks in a BCI implementation.

Across participants, selected current sources were distributed largely across the primary somatosensory cortex (Brodmann areas 1, 2 and 3), the primary motor cortex (Brodmann area 4), the premotor cortex and supplementary motor area (Brodmann area 6), the inferior parietal cortex (IPC) and the lateral operculum (OP3 and OP4). The activations in Brodmann areas 1, 2, 3, 4 and 6 were expected since these are well-known areas that contribute to motor planning and execution. Activations in the rostral and middle areas of the IPC, and the OP3 and OP4, although not expected, were reasonable considering these are adjacent to the sensorimotor areas and the inverse and forward normalization processes (adjustment of individual brain coordinates to a standard brain model, and vice versa) is not a perfect process. However, the IPC, OP3 and OP4 may have also shown activation in relation to the experimental tasks. Studies by (Caspers et al., 2011, 2013) have suggested that the rostral areas of IPC are functionally connected to the motor, premotor and somatosensory areas in the brain, and the current sources activated in the rostral IPC, may be related to the sensorimotor integration of experimental motor tasks observation and execution. Activation in middle IPC may have arisen as a result of the fixation crosses used in the EEG experiment, since this area is involved with visually guided attention. The OP3 and OP4 are part of the secondary somatosensory cortex and studies have reported activations in these areas as a result of walking related somatosensory stimulations (Labriffe, et al., 2017; Disbrow, et al., 2000; Eickhoff, et al., 2007).

Finally, the contribution of Brodmann areas 4 and 6 was also studied since these areas have strong activations during the execution of motor tasks, and therefore were expected to have a high contribution to the classification accuracies. The Brodmann area 4 contains the primary motor cortex, and the commands generated in this area are more closely related to the mechanical details of the movement and are usually less influenced by the behavioral context. In contrast, the activation in Brodmann area 6, which contains the premotor cortex and the supplementary motor cortex, is more dependent on the context in which the action is performed, and it may be involved in organizing or planning the sequence of muscle activation for a movement (Kandel, et al., 2013).

The results showed in Figure 22 for the 9-classes classification using only current sources vertices in Brodmann areas 4 and 6 separately, showed accuracies higher than chance level (current sources area 4: 58.14% ±5.58, p = 2.99e-04; area 6: 50.72% ±5.43, p = 2.99e-04) and there was no significant difference between both accuracies. The high contribution of the Brodmann area 4 was expected considering the active experimental tasks. On the other hand, the contribution of Brodmann area 6 may be related to the specific directions required for the execution of each of the 9 experimental tasks: the participants needed to plan a movement that involved only the right or the left leg, a flexion or extension of the ankles, and a force level. It is important to consider that neither of the voxels concentrated in only Brodmann area 4 or Brodmann area 6, could achieve the same classification accuracy to the accuracy obtained when all the Brodmann areas of interest together were included in the analysis. Future connectivity analyses could enlighten the interaction of these areas during ankle movements.

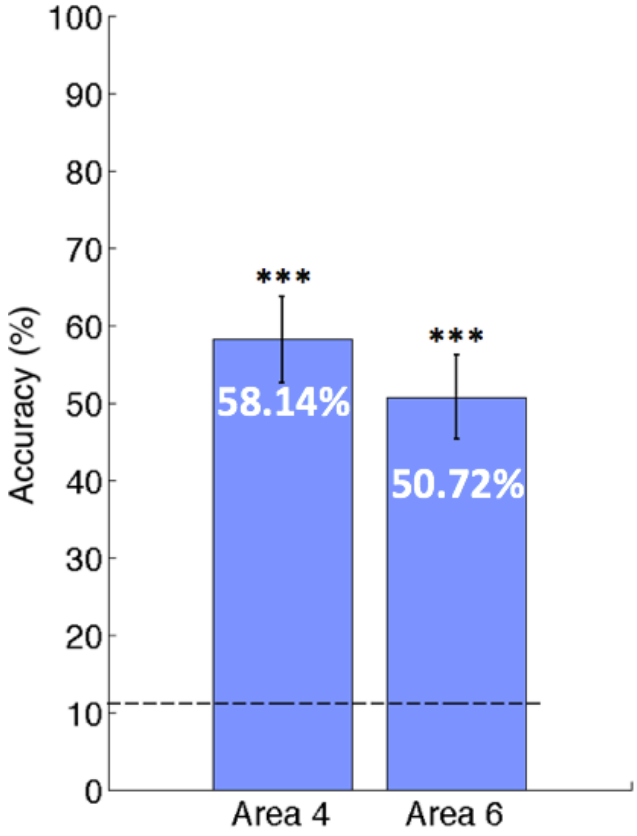

Figure 22 – Classification accuracies obtained for the 9-class decoding using only the estimated current sources located in Brodmann areas 4 and 6 separately.

Chapter 4: Effect of the Reducing Number of EEG Electrodes on the Classification Accuracy

To study the feasibility of taking a BCI outside the laboratory, it is important to consider technical aspects such as the EEG electrodes configuration. In this chapter we study the accuracy of our decoder with different number of EEG electrodes, with the purpose of evaluating the minimum number of electrodes that could be used to achieve high classification accuracies.

Using a lower number of electrodes could encourage the future BCI user into integrating the BCI in their daily living, as well as patients with reduced mobility in their upper limbs can also benefit from the reduced setting up time. Additionally, we aim to reduce the parameter tuning time of the decoder, by using only the structural MRI data for current source estimation. This means that no fMRI information will be included to create area and activity priors used for the current source estimation, and instead we will use the whole cortex and a uniform distribution for current sources intensity.

For the analysis described in this chapter, only the brain model and the EEG data were used and the fMRI information was not included.

4.1. Current Source Estimation Parameters

Current sources estimation was done similarly as described in section 3.1 Current Source Estimation Parameters, however the EEG signals used as inputs in this chapter 4 were further cleaned for artifacts using ICA (see 2.5.2 EEG Preprocessing for Chapter 4 - EEG Data Preprocessing).

For the current variance and the inverse filter estimation, no hierarchical prior of area and activity from fMRI information was used, meaning the current sources were estimated all over the cortex and the activity was assumed as uniform for all vertices (Figure 23). The segment of 0.5 to 0 s of each EEG trial was used as baseline, and the epoch from 0.5 s to 3 s, was divided into 14 windows of 0.5 s of length each, overlapping for 0.25 s. Dipole reduction ratios were set individually for each participant to reduce the number of vertices from 10,004 to 200. These parameters were used for current variance, inverse filter and current source estimation. The obtained current source time-series were used as input for the classifier.

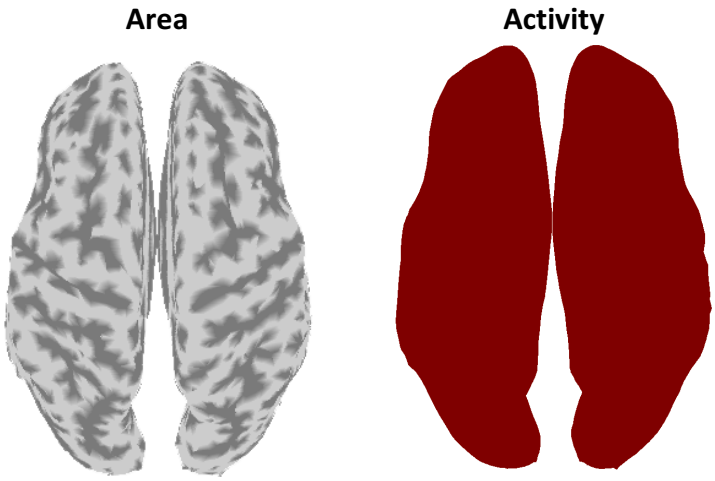

Figure 23 – The whole cortex model and the uniform activity, were used for the estimation.

4.2. Classification of EEG and Estimated Cortical Current Sources

Classification of estimated current sources and preprocessed EEG sensor time-series, was done as described in chapter 3.2: Input signals were resampled down to 30 Hz and the epoch from 0 s to 1 s (different from the epoch from 0 s to 0.5 s used in chapter 3) were used as inputs for the SLR classifier. Downsampled time-series signals were classified using a LOO method, and mean classification accuracies were obtained for each of the 9-class classification. The classification was performed separately for each of the EEG sensor configurations shown in Figure 24.

4.3. Results and Discussion

Obtained accuracies for each sensor configuration and confusion tables are shown in Figure 24, and Tables 5 – 8. Accuracies from both current sources classification and EEG were significantly higher than chance level (11.11% for 9-class classification). Current sources: 32 sensors: 65.50% ±4.24, p = 5.40e-04; 16 sensors: 62.39% ±3.40, p = 5.40e-04; 8 sensors (1): 57.75% ±2.37, p = 5.29e-04; 8 sensors (2): 45.17 ±3.07, p = 5.29e-04; EEG: 32 sensors: 20.08% ±1.39, p = 5.29e-04; 16 sensors: 18.67% ±1.14, p = 5.40e-04; 8 sensors (1): 18.69% ±0.90, p = 5.29e-04; 8 sensors (2): 14.03% ±0.79, p = 5.40e-04, p-values corrected for multiple comparisons using a FDR of 0.05.

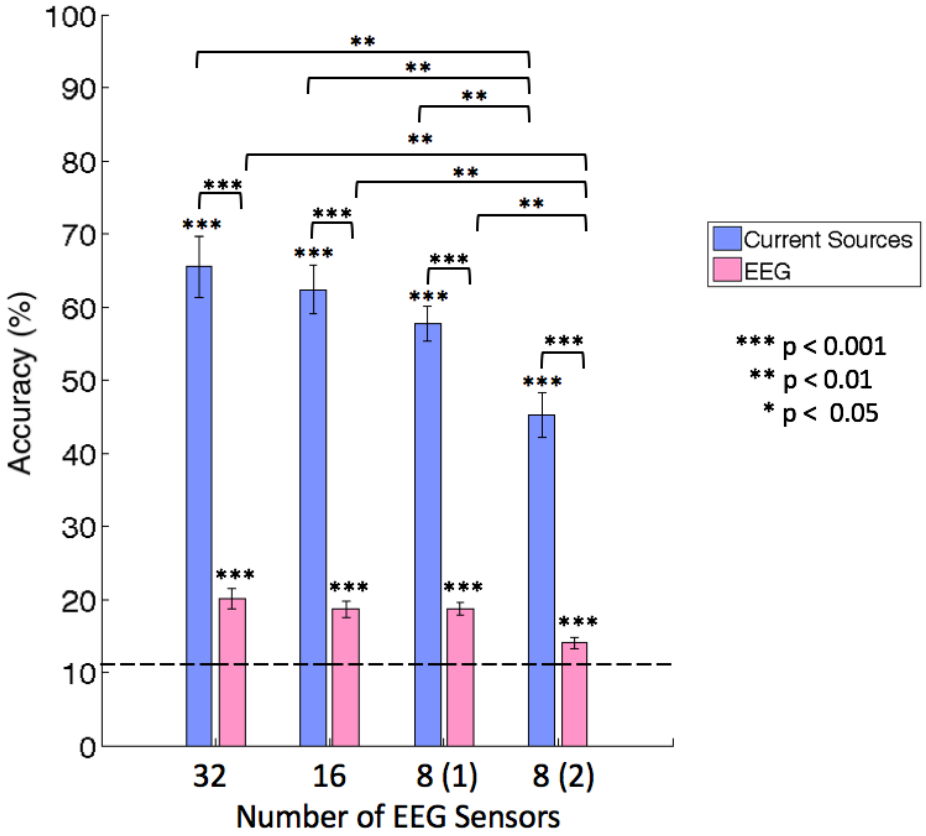

Figure 24 – Classification accuracies obtained for the 4 configurations of EEG electrodes.

As expected, the classification accuracy decreased when the number of EEG sensors also decreased, however a significant difference was found only between the 8(2) sensors configuration and the other configurations, for both current sources and EEG. Even though there were two different configurations of 8 sensors each (8(1) and 8(2)), a significant difference was found between them suggesting that the position of the EEG sensors over the scalp has a high influence on the estimation of current sources. The complex geometry of sulci and gyri in the brain seems to have a "dispersion" effect of electric potentials that was larger than expected. Even though electric potentials may be generated in a specific ROI, these potentials are widely distributed across the brain cortex and the EEG electrodes concentrated over the ROI cannot provide enough information for current source estimation with VBMEG, when there is a lack of prior information of area and activity.

Target \ Selected	HLD	HLU	HRD	HRU	LLD	LLU	LRD	LRU	Still
HLD	33.50	2.38	2.38	1.63	1.63	1.63	1.38	2.63	2.88
HLU	3.38	31.50	1.38	2.00	3.63	3.00	1.25	1.00	2.88
HRD	2.50	2.25	34.13	1.88	1.50	2.25	2.25	1.88	1.38
HRU	0.38	1.25	2.25	36.63	1.75	1.38	3.25	1.63	1.50
LLD	1.50	2.13	1.00	1.88	33.38	4.50	0.88	2.75	2.00
LLU	2.38	2.25	1.88	2.13	4.38	30.25	1.75	2.88	2.13
LRD	1.38	1.88	2.88	4.00	1.75	1.88	30.88	3.75	1.63
LRU	1.75	1.75	2.63	1.63	1.88	2.63	3.50	31.75	2.50
Still	1.88	2.63	1.63	2.25	2.00	2.00	1.75	3.13	32.75
Class Accuracy (%)	67 ± 2.64	63 ± 2.78	68.25 ± 2.35	73.25 ± 2.40	66.75 ± 3.87	60.5 ± 4.01	61.75 ± 1.87	63.5 ± 3.10	65.5 ± 2.64
Average Accuracy (%)	65.5 ± 4.24								

Table 5 – Averaged confusion table across trials and participants, for the classification of current sources in the 32 EEG sensor configuration

Selected / Target	HLD	HLU	HRD	HRU	LLD	LLU	LRD	LRU	Still
HLD	31.13	2.50	4.50	2.13	2.25	2.13	1.75	1.88	1.75
HLU	3.00	32.00	2.75	2.38	2.50	1.75	1.88	1.75	2.00
HRD	3.50	1.63	31.88	2.00	1.88	1.88	2.38	3.13	1.75
HRU	2.25	3.13	2.38	29.63	2.38	1.75	3.38	4.38	0.75
LLD	2.88	1.63	1.75	2.13	31.00	3.88	2.63	2.75	1.38
LLU	2.00	1.38	2.38	1.50	2.50	33.25	1.50	4.00	1.50
LRD	2.50	1.63	2.00	3.63	3.00	1.38	29.38	4.38	2.13
LRU	2.63	1.75	2.25	5.00	2.38	2.25	2.50	29.38	1.88
Still	1.63	1.50	1.88	2.13	2.50	2.63	2.75	1.88	33.13
Class Accuracy (%)	62.25 ± 3.39	64 ± 3.19	63.75 ± 2.75	59.25 ± 2.56	62 ± 2.89	66.5 ± 2.88	58.75 ± 1.79	58.75 ± 2.96	66.25 ± 2.61
Average Accuracy (%)	62.39 ± 3.40								

Table 6 – Averaged confusion table across trials and participants, for the classification of current sources in the 16 EEG sensor configuration

Selected / Target	HLD	HLU	HRD	HRU	LLD	LLU	LRD	LRU	Still
HLD	29.75	2.00	3.13	1.75	3.13	1.38	1.75	3.25	3.88
HLU	1.63	29.88	2.13	2.75	1.75	3.75	3.38	3.50	1.25
HRD	3.00	2.75	26.75	4.00	3.00	1.88	3.00	3.75	1.88
HRU	2.00	2.25	5.00	27.38	1.63	1.13	2.75	5.38	2.50
LLD	3.50	1.75	2.63	2.38	30.38	2.50	1.75	3.38	1.75
LLU	0.88	6.00	0.75	1.88	3.75	29.25	2.50	2.50	2.50
LRD	2.63	3.75	2.13	3.38	1.13	2.13	29.63	3.25	2.00
LRU	2.38	2.25	3.63	3.38	2.63	1.75	2.75	28.63	2.63
Still	3.75	2.75	1.63	2.63	3.13	1.38	2.50	4.00	28.25
Class Accuracy (%)	59.5 ± 2.26	59.75 ± 1.76	53.5 ± 1.78	54.75 ± 2.66	60.75 ± 1.79	58.5 ± 2.91	59.25 ± 1.89	57.25 ± 2.16	56.5 ± 1.63
Average Accuracy (%)	57.75 ± 2.37								

Table 7 – Averaged confusion table across trials and participants, for the classification of current sources in the 8 (1) EEG sensor configuration

Selected / Target	HLD	HLU	HRD	HRU	LLD	LLU	LRD	LRU	Still
HLD	22.88	3.25	4.00	3.63	3.75	3.00	2.63	2.25	4.63
HLU	3.63	27.13	2.25	4.00	3.13	2.75	1.63	2.25	3.25
HRD	3.63	2.75	20.38	4.00	2.63	4.25	4.88	3.00	4.50
HRU	3.63	2.88	3.13	23.88	2.63	2.25	3.38	2.63	5.63
LLD	4.38	2.25	2.88	3.38	22.00	4.38	2.63	4.38	3.75
LLU	3.63	1.63	4.00	1.63	6.00	23.13	3.38	3.13	3.50
LRD	3.13	3.38	3.13	3.50	3.13	4.00	20.63	5.13	4.00
LRU	1.63	1.38	3.63	3.75	3.13	4.25	5.13	22.00	5.13
Still	4.13	2.38	4.25	2.63	4.00	4.00	3.25	4.13	21.25
Class Accuracy (%)	45.75 ± 2.64	54.25 ± 2.39	40.75 ± 1.61	47.75 ± 2.20	44 ± 3.90	46.25 ± 2.17	41.25 ± 2.08	44 ± 2.60	42.5 ± 2.42
Average Accuracy (%)	45.17 ± 3.07								

Table 8 – Averaged confusion table across trials and participants, for the classification of current sources in the 8 (2) EEG sensor configuration

An analysis of the weights assigned by the classifier to time-points of current sources and EEG sensor signals was also performed. The weights were averaged across time-points and trials for each task and plotted on the cortical model of each participant. However, since in this study all the cortical area was used, and no prior information for area and activity was given, the weight analysis showed contributive vertices distributed all over the brain cortex.

In order to obtain physiologically acceptable results in from the classifier, it is essential to include high-resolution prior information from techniques such as fMRI or near infrared spectroscopy (NIRS) in the current source estimation with VBMEG.

The specifications for current estimation used in this chapter are focused towards an alternative for a brain decoder from the engineering point of view, that does not require prior knowledge of the activation of specific brain areas to yield current sources that can be classified with high accuracies. This approach could benefit the future BCI users that are unable to spend long sessions in an MRI scanner (i.e., children or patients with claustrophobia), or have intact brain function, because the decoder could be tuned faster by using a standard brain model and the acquired EEG data.

The successful implementation of this decoder into a real-time BCI depends on various factors, including using a shorter time window for decoding and training of the BCI user into modulating their brain signals, however using the lower number of EEG electrodes possible while obtaining high classification accuracies, is crucial for a faster estimation of the inverse filter and a faster set up for the BCI user. Based on the results presented in this chapter, we suggest the use of at least 8 electrodes distributed in the configuration 8(1) for to design decoders for BCIs based on walking-related tasks to control exoskeletons or neuroprosthesis.

Chapter 5: General Discussion

5.1. Conclusions

The study described in this manuscript successfully created decoders for the classification of walking related tasks using non-invasive brain recordings. To our knowledge, this study is the first to classify 8 active walking-related motor tasks and 1 control task from non-invasive EEG recordings using a distributed current source method.

In chapter 3, EEG and fMRI recordings were used for the decoder. The fMRI information was imposed as a prior of area (ROI) and activity (t-values from fMRI), concentrated on the brain areas well known for contributing to motor planning and execution. Furthermore, the priors used were obtained from a second-level (group) analysis, which could benefit the patients that cannot spend long sessions in the MRI scanner.

In chapter 4 a more generalized approach was used, as only the structural images of the brain and the EEG information was used for estimating current sources all over the brain cortex. Different numbers and configurations of EEG electrodes were tested, in order to suggest the minimum number of EEG electrodes that could be used to obtain high classification accuracies for the 9-class decoding.

The goal of this study is to provide an insight of a decoder that can be implemented in the future development of a BCI, that can benefit patients with reduced motor control, specifically patients with walking impairments, as hemiplegia and paraplegia, caused by stroke and spinal cord injury respectively.

The main question in chapter 3 was whether it was possible to decode walking related to tasks using only current sources estimated from the related brain areas. As an answer, 9 classes could be successfully classified with an accuracy of 65.64%. As for chapter 4, the question of how does the number of EEG electrodes affect the decoding accuracy when no fMRI prior is used, was addressed. Using configurations of 32, 16 and 8 EEG sensors, we obtained the highest classification accuracy for 32 sensors (65.50%), however a non-significant difference was found with the 8(1) sensor configuration, which achieved an accuracy of 57.75%. Even though the classification is lower, it suggests that with further parameter tuning the 8(1) EEG sensor configuration might be suitable for BCI application.

Finally, the approach in chapter 3 could benefit patients with hemiplegia caused by stroke, as their brain will go through a plasticity process of creating new neural connections trying to compensate for the lost functions. The use of fMRI could detect these plasticity changes and since this information is integrated to VBMEG for current source estimation, we could obtain

personalized brain activation patterns related to a specific motor task. On the other hand, the approach in chapter 4 could benefit patients with paraplegia caused by spinal cord injury, as the brain remains intact and therefore setting a decoder for a BCI could be faster and more practical since prior information from fMRI might not be required, and the computation of the inverse filters is faster for lower number of electrodes.

Limitations and challenges

Ideally, the mean accuracy of a BCI decoder across participants should surpass a 70% accuracy threshold with a chance level of 50% (Pfurtscheller, et al., 2005). Extending this threshold to the multiclass problem, it becomes necessary to increase the classification accuracy before moving on to an online BCI. One possible approach to increase the accuracy is to use different fMRI priors that are specific for each task: area and activity priors are obtained from statistical parametric maps generated for specific contrasts. In this study, these maps were generated for "all left leg tasks" and "all right leg tasks" and merged into one contrast, from which one common activity prior and one common area prior were obtained and used for current source estimation of all tasks. Instead of obtaining one contrast, it is possible to obtain one contrast (and therefore area and activity priors) per task. In total, 9 sets of priors (area and activity) corresponding to each experimental task could be used to estimate inverse filters for each task separately. This could increase the classification accuracy to the cost of increased time in designing the decoder.

Ideally, one generalized filter that could be used across sessions would be desirable, however the inverse filter and the classifier still need to be estimated for every session. Training of the decoder user to teach them how to elicit the brain rhythms that remain similar through sessions could significantly improve the accuracy, however this is still to be tested for our methodology.

Estimating current sources in VBMEG with the default parameters of the toolbox is acceptable and good results can be achieved, however depending on the tasks of interest and each participant, the personalized combination of different parameters may improve the current source estimation performance (i.e., different hyperparameters combinations if priors are used, or different radius for the smoothness filter parameter).

Another question to address is the application of the methodologies described in this manuscript, to the classification of motor imagery tasks of users with highly restricted mobility, as in the case of users with complete spinal cord injuries.

Finally, good classification accuracies were obtained when 1 second of data was used as input for the classifier, however for the online and real-time BCI, efforts should be made to obtain high accuracies using a substantially smaller epoch of current sources time-series.

5.2. Future Work

To continue with the development of a more generalized decoder for walking, it is recommended to apply the methodologies described in this manuscript with two approaches for current estimation: 1) applying the area and activity priors obtained from the group analysis performed here, to new participants not included in the fMRI analysis, and 2) using a standard model of the brain. If high classification accuracies can be obtained with these two approaches, then MRI and fMRI experiments might be omitted for the design of the decoder, and patients with some type of contraindication to the use of the MRI scanner could also benefit.

Towards an online BCI

The methods described here are applicable to real-time interfaces, since the inverse filters and the decoders can be estimated beforehand. Figure 25 shows a proposed design for an online BCI. MRI and fMRI could be acquired anytime before the decoder estimation; however, EEG should be recorded the same day.

The first step would be the preprocessing of the MRI and fMRI data (when available) to obtain area and activity priors for the current source estimation. This information should be ready by the day the online BCI session would be carried out. On the session day, an EEG session performing the walking-related tasks should be performed, along with the EEG electrodes positions acquisition. The priors, the electrodes position and the preprocessed EEG data could then used to estimate the inverse filter and the current sources. At this point it is worth mentioning that different strategies could be used for inverse filter estimation, for example, estimating one filter common for all tasks, or estimating one filter per task. The inverse filter would be used later in the online BCI, while the estimated current sources are used to train the classifier. From the classifier, a weight matrix corresponding to the number of features by the number of classes is obtained. This concludes the offline part.

For the online step, the short windows of acquired EEG data are preprocessed and fed into the current source estimation module, along with the previously estimated inverse filter. The obtained current sources are then used as inputs for the SLR decoder along with the matrix of weights obtained from the offline analysis. As a result, the SLR classifier will assign probabilities to each task and the task with the highest probability is selected as the output of the BCI.

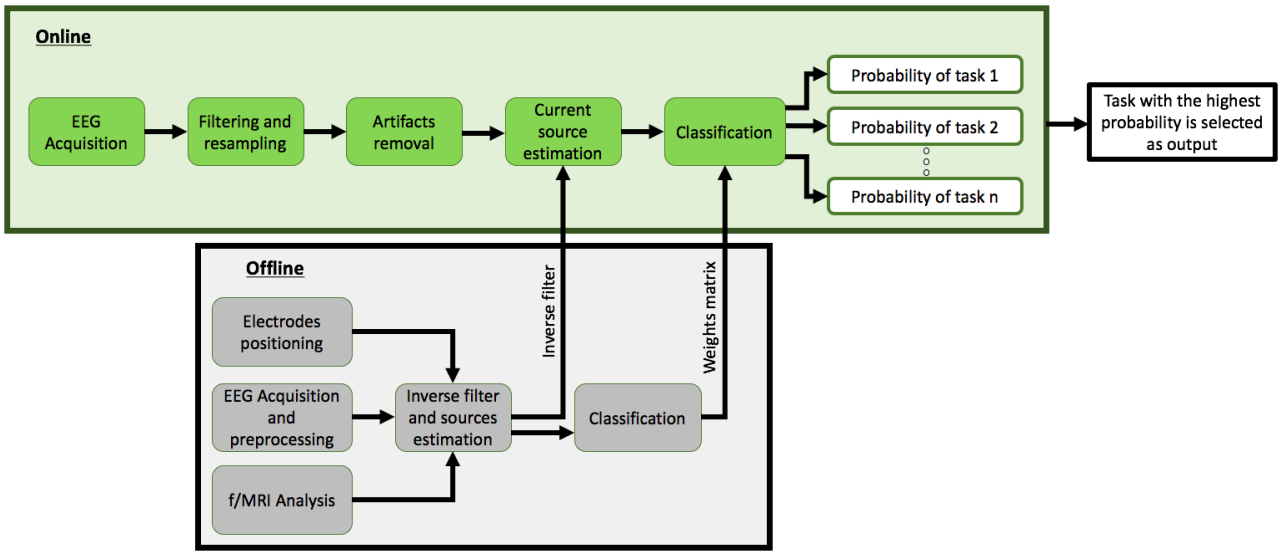

Figure 25 – Proposed design for an online BCI based on the current source estimation with VBMEG and the classification with sparse logistic regression

While Figure 25 describes a general approach for an online BCI, it is important to consider that training and feedback are necessary for a successful implementation. For the actual motor task execution, it could be the case where the inverse filter estimation has to be done only once at the beginning of the online BCI session, however in the case of imagery (kinesthetic imagination of motor tasks), the BCI user has to be trained to produce brain rhythms that remain similar for specific motor tasks throughout sessions.

BCI literacy is achieved when the BCI user's performances reaches at least 70% accuracy, therefore it is necessary first to increase the accuracy of the decoder. After this accuracy is achieved, the decoder could be tested in online environments to finally being applied to control exoskeletons or neuroprosthesis for walking. Existing devices and BCIs for walking assistance, detect walking intention and then trigger a pre-established walking sequence, however if 9 walking-related tasks could be decoded successfully in an online and real-time BCI, then the BCI user will have a more natural control over the walking sequence.

Related Publications

Mejia Tobar A, Hyoudou R, Kita K, Nakamura T, Kambara H, Ogata Y, Hanakawa T, Koike Y and Yoshimura N (2018) Decoding of Ankle Flexion and Extension from Cortical Current Sources Estimated from Non-invasive Brain Activity Recording Methods. Front. Neurosci. 11:733. doi: 10.3389/fnins.2017.00733

Mejia Tobar A, Kita K, Nakamura T, Kambara H, Ogata Y, Hanakawa T, Koike Y and Yoshimura N (2018) Effect of the EEG Sensor Number on the Current-Source Decoder Performance based on a variational Bayesian method (VBMEG). International Journal of Engineering Research and Allied Sciences (IJERAS) 3:5.

References

Aihara, T., Takeda, Y., Takeda, K., Yasuda, W., Sato, T., Otaka, Y., et al. (2012). Cortical current source estimation from electroencephalography in combination with near-infrared spectroscopy as a hierarchical prior. Neuroimage. doi:10.1016/j.neuroimage.2011.09.087.

Ashby, G. Statistical Analysis of fMRI data. MIT Press.

Baldi, J. C., Jackson, R. D., Moraille, R., and Mysiw, W. J. (1998). Muscle atrophy is prevented in patients with acute spinal cord injury using functional electrical stimulation. Spinal Cord. doi:10.1038/sj.sc.3100679.

Bishop, C. M. (2006). Pattern Recognition and Machine Learning. doi:10.1117/1.2819119.

Boncompagni, S. (2012). Severe muscle atrophy due to spinal cord injury can be reversed in complete absence of peripheral nerves. Eur. J. Transl. Myol. -Basic Appl. Myol.

Boser, B. E., Guyon, I. M., and Vapnik, V. N. (1992). A training algorithm for optimal margin classifiers. in Proceedings of the fifth annual workshop on Computational learning theory - COLT '92 doi:10.1145/130385.130401.

Carmena, J. M., Lebedev, M. A., Crist, R. E., O'Doherty, J. E., Santucci, D. M., Dimitrov, D. F., et al. (2003). Learning to control a brain-machine interface for reaching and grasping by primates. PLoS Biol. doi:10.1371/journal.pbio.0000042.

Carraro, U., Kern, H., Gava, P., Hofer, C., Loefler, S., Gargiulo, P., et al. (2015). Biology of muscle atrophy and of its recovery by FES in aging and mobility impairments: roots and by-products. Eur. J. Transl. Myol. doi:10.4081/ejtm.2015.5272.

Caspers, S., Eickhoff, S. B., Rick, T., von Kapri, A., Kuhlen, T., Huang, R., et al. (2011). Probabilistic fibre tract analysis of cytoarchitectonically defined human inferior parietal lobule areas reveals similarities to macaques. Neuroimage 58, 362–380. doi: 10.1016/j.neuroimage.2011.06.027

Caspers, S., Schleicher, A., Bacha-Trams, M., Palomero-Gallagher, N., Amunts, K., and Zilles, K. (2013). Organization of the human inferior parietal lobule based on receptor architectonics. Cereb. Cortex 23, 615–628. doi: 10.1093/cercor/bhs048

Dale, A. M., Liu, A. K., Fischl, B. R., Buckner, R. L., Belliveau, J. W., Lewine, J. D., et al. (2000). Dynamic statistical parametric mapping: Combining fMRI and MEG for high-resolution imaging of cortical activity. Neuron. doi:10.1016/S0896-6273(00)81138-1.

Disbrow, E., Roberts, T., and Krubitzer, L. (2000). Somatotopic organization of cortical fields in the lateral sulcus of Homo sapiens: evidence for SII and PV. J. Comp. Neurol. 418, 1–21. doi: 10.1002/(SICI)1096-9861(20000228)418:1<1::AID-CNE1>3.0.CO;2-P
Eickhoff, S. B., Grefkes, C., Zilles, K., and Fink, G. R. (2007). The somatotopic organization of cytoarchitectonic areas on the human parietal operculum. Cereb. Cortex 17, 1800–1811. doi: 10.1093/cercor/bhl090

Eickhoff, S. B., Stephan, K. E., Mohlberg, H., Grefkes, C., Fink, G. R., Amunts, K., et al. (2005). A new SPM toolbox for combining probabilistic cytoarchitectonic maps and functional imaging data. Neuroimage. doi:10.1016/j.neuroimage.2004.12.034.

Ferrante, S., Bejarano, N. C., Ambrosini, E., Nardone, A., Turcato, A. M., Monticone, M., et al. (2016). A personalized multi-channel FES controller based on muscle synergies to support gait rehabilitation after stroke. Front. Neurosci. doi:10.3389/fnins.2016.00425.

Fitzsimmons, N. A. (2009). Extracting kinematic parameters for monkey bipedal walking from cortical neuronal ensemble activity. Front. Integr. Neurosci. doi:10.3389/neuro.07.003.2009.

Furnham, A., and Thompson, R. (1994). Actual and perceived attitudes of wheelchair users. Couns. Psychol. Q. 7, 35–51. doi:10.1080/09515079408254133.

Galli, G., Lenggenhager, B., Scivoletto, G., Molinari, M., and Pazzaglia, M. (2015). Don't look at my wheelchair! The plasticity of longlasting prejudice. Med. Educ. doi:10.1111/medu.12834.

Hämäläinen, M., Hari, R., Ilmoniemi, R. J., Knuutila, J., and Lounasmaa, O. V. (1993). Magnetoencephalography theory, instrumentation, and applications to noninvasive studies of the working human brain. Rev. Mod. Phys. doi:10.1103/RevModPhys.65.413.

Hashimoto, Y., and Ushiba, J. (2013). EEG-based classification of imaginary left and right foot movements using beta rebound. Clin. Neurophysiol. doi:10.1016/j.clinph.2013.05.006.

Hochberg, L. R., Bacher, D., Jarosiewicz, B., Masse, N. Y., Simeral, J. D., Vogel, J., et al. (2012). Reach and grasp by people with tetraplegia using a neurally controlled robotic arm. Nature. doi:10.1038/nature11076.

Jiang, N., Gizzi, L., Mrachacz-Kersting, N., Dremstrup, K., and Farina, D. (2015). A brain-computer interface for single-trial detection of gait initiation from movement related cortical potentials. Clin. Neurophysiol. doi:10.1016/j.clinph.2014.05.003.

Kandel, E. R., Schwartz, J. H., Jessell, T. M., Siegelbaum, S. A., and Hudspeth, A. J. (2014). Principles of Neural Science, Fifth Edition. doi:10.1036/0838577016.

King, C. E., Wang, P. T., McCrimmon, C. M., Chou, C. C., Do, A. H., and Nenadic, Z. (2015). The feasibility of a brain-computer interface functional electrical stimulation system for the restoration of overground walking after paraplegia. J. Neuroeng. Rehabil. doi:10.1186/s12984-015-0068-7.

Kybic, J., Clerc, M., Faugeras, O., Keriven, R., and Papadopoulo, T. (2006). Generalized head models for MEG/EEG: Boundary element method beyond nested volumes. Phys. Med. Biol. doi:10.1088/0031-9155/51/5/021.

Labriffe, M., Annweiler, C., Amirova, L. E., Gauquelin-Koch, G., Ter Minassian, A., Leiber, L.-M., et al. (2017). Brain activity during mental imagery of gait versus gait-like plantar stimulation: a novel combined functional MRI paradigm to better understand cerebral gait control. Front. Hum. Neurosci. 11:106. doi: 10.3389/fnhum.2017.00106

Li, S. (2017). Spasticity, motor recovery, and neural plasticity after stroke. Front. Neurol. doi:10.3389/fneur.2017.00120.

Mak, J. N., and Wolpaw, J. R. (2009). Clinical Applications of Brain—Computer Interfaces: Current State and Future Prospects. IEEE Rev. Biomed. Eng. doi:10.1109/RBME.2009.2035356.

Meng, L., Porr, B., Macleod, C. A., and Gollee, H. (2017). A functional electrical stimulation system for human walking inspired by reflexive control principles. Proc. Inst. Mech. Eng. Part H J. Eng. Med. doi:10.1177/0954411917693879.

Morioka, H., Kanemura, A., Morimoto, S., Yoshioka, T., Oba, S., Kawanabe, M., et al. (2014). Decoding spatial attention by using cortical currents estimated from electroencephalography with near-infrared spectroscopy prior information. Neuroimage. doi:10.1016/j.neuroimage.2013.12.035.

Neal, R.M., 1996. Bayesian Learning for Neural Networks. Springer Verlag, New York.

Negård, N. O., Schauer, T., Kauert, R., and Raisch, J. (2006). An FES-assisted gait training system for hemiplegic stroke patients based on inertial sensors. in IFAC Proceedings Volumes (IFAC-PapersOnline) doi:10.3182/20060920-3-FR-2912.00058.

Nichols, T., and Holmes, A. (2003). “Nonparametric Permutation Tests for Functional Neuroimaging,” in Human Brain Function: Second Edition doi:10.1016/B978-012264841-0/50048-2.

Pascual-Marqui, R. D. (2002). Standardized low-resolution brain electromagnetic tomography (sLORETA): technical details. Methods Find. Exp. Clin. Pharmacol. doi:841 [pii].

Pascual-Marqui, R. D. (2007). Discrete, 3D distributed, linear imaging methods of electric neuronal activity. Part 1: exact, zero error localization. Clin. Neurophysiol. doi:10.1016/S1388-2457(00)00546-0.

Pascual-Marqui, R. D., Michel, C. M., and Lehmann, D. (1994). Low resolution electromagnetic tomography: a new method for localizing electrical activity in the brain. Int. J. Psychophysiol. doi:10.1016/0167-8760(84)90014-X.

Pazzaglia, M., and Molinari, M. (2016). The embodiment of assistive devices-from wheelchair to exoskeleton. Phys. Life Rev. doi:10.1016/j.plrev.2015.11.006.

Pereira, J., Ofner, P., Schwarz, A., Sburlea, A. I., and Müller-Putz, G. R. (2017). EEG neural correlates of goal-directed movement intention. Neuroimage. doi:10.1016/j.neuroimage.2017.01.030.

Perry, J. (1992). Gait Analysis - Normal and Pathological Function. pp. 3 – 15, 52 – 60. doi:10.1017/CBO9781107415324.004.

Pfurtscheller, G., Neuper, C., and Birbaumer, N. (2005). Human Brain-Computer Interface. Mot. Cortex Volunt. Movements.

Robinson, N., Guan, C., Vinod, A. P., Keng Ang, K., and Peng Tee, K. (2013). Multi-class EEG classification of voluntary hand movement directions. J. Neural Eng. doi:10.1088/1741-2560/10/5/056018.

Russell, S. J., and Norvig, P. (1995). Artificial Intelligence: A Modern Approach. doi:10.1016/0925-2312(95)90020-9.

Sato, M., Yoshioka, T., Kajihara, S., Toyama, K., Goda, N., Doya, K., et al. (2004). Hierarchical Bayesian estimation for MEG inverse problem. Neuroimage. doi:10.1016/j.neuroimage.2004.06.037.

Schwarz, A., Ofner, P., Pereira, J., Sburlea, A. I., and Müller-Putz, G. R. (2018). Decoding natural reach-and-grasp actions from human EEG. J. Neural Eng. doi:10.1088/1741-2552/aa8911.

Severens, M., Perusquia-Hernandez, M., Nienhuis, B., Farquhar, J., and Duysens, J. (2015). Using actual and imagined walking related desynchronization features in a BCI. IEEE Trans. Neural Syst. Rehabil. Eng. doi:10.1109/TNSRE.2014.2371391.

Silva, C., Maltez, J. C., Trindade, E., Arriaga, A., and Ducla-Soares, E. (2004). Evaluation of L1and L2minimum norm performances on EEG localizations. Clin. Neurophysiol. doi:10.1016/j.clinph.2004.02.009.

Singh, S. P. (2014). Magnetoencephalography: Basic principles. Ann. Indian Acad. Neurol. 17, S107–S112. doi:10.4103/0972-2327.128676.

Stockton, L., and Parker, D. (2002). Pressure relief behaviour and the prevention of pressure ulcers in wheelchair users in the community. J. Tissue Viability. doi:10.1016/S0965-206X(02)80031-6.

Taylor, D. M., Tillery, S. I. H., and Schwartz, A. B. (2002). Direct cortical control of 3D neuroprosthetic devices. Science. doi:10.1126/science.1070291.

Vapnik, V. N. (1999). An overview of statistical learning theory. IEEE Trans. Neural Netw. doi:10.1109/72.788640.

Velliste, M., Perel, S., Spalding, M. C., Whitford, A. S., and Schwartz, A. B. (2008). Cortical control of a prosthetic arm for self-feeding. Nature. doi:10.1038/nature06996.

Weingarden, H., and Ring, H. (2006). Functional electrical stimulation-induced neural changes and recovery after stroke. Eura. Medicophys.

Wessberg, J., Stambaugh, C. R., Kralik, J. D., Beck, P. D., Laubach, M., Chapin, J. K., et al. (2000). Real-time prediction of hand trajectory by ensembles of cortical neurons in primates. Nature. doi:10.1038/35042582.

Wolpaw, J. R., Birbaumer, N., McFarland, D. J., Pfurtscheller, G., and Vaughan, T. M. (2002). Brain-computer interfaces for communication and control. Clin. Neurophysiol. doi:10.1016/S1388-2457(02)00057-3.

Wolpaw, J. R., Birbaumer, N., McFarland, D. J., Pfurtscheller, G., and Vaughan, T. M. (2002). Brain-computer interfaces for communication and control. Clin. Neurophysiol. doi:10.1016/S1388-2457(02)00057-3.

Xu, R., Jiang, N., Mrachacz-Kersting, N., Lin, C., Asin Prieto, G., Moreno, J. C., et al. (2014). A closed-loop brain-computer interface triggering an active ankle-foot orthosis for inducing cortical neural plasticity. IEEE Trans. Biomed. Eng. doi:10.1109/TBME.2014.2313867.

Yamashita, O., Sato, M. A., Yoshioka, T., Tong, F., and Kamitani, Y. (2008). Sparse estimation automatically selects voxels relevant for the decoding of fMRI activity patterns. Neuroimage. doi:10.1016/j.neuroimage.2008.05.050.

Yoshimura, N., DaSalla, C. S., Hanakawa, T., Sato, M. aki, and Koike, Y. (2012). Reconstruction of flexor and extensor muscle activities from electroencephalography cortical currents. Neuroimage. doi:10.1016/j.neuroimage.2011.08.029.

Yoshimura, N., Nishimoto, A., Belkacem, A. N., Shin, D., Kambara, H., Hanakawa, T., et al. (2016). Decoding of covert vowel articulation using electroencephalography cortical currents. Front. Neurosci. doi:10.3389/fnins.2016.00175.

Yoshimura, N., Tsuda, H., Kawase, T., Kambara, H., and Koike, Y. (2017). Decoding finger movement in humans using synergy of EEG cortical current signals. Sci. Rep. doi:10.1038/s41598-017-09770-5.

Yoshioka, T., Toyama, K., Kawato, M., Yamashita, O., Nishina, S., Yamagishi, N., et al. (2008). Evaluation of hierarchical Bayesian method through retinotopic brain activities reconstruction from fMRI and MEG signals. Neuroimage. doi:10.1016/j.neuroimage.2008.06.013.

Zander, T. O., Kothe, C., Welke, S., and Roetting, M. (2009). Utilizing secondary input from passive brain-computer interfaces for enhancing human-machine interaction. in Lecture Notes in Computer Science (including subseries Lecture Notes in Artificial Intelligence and Lecture Notes in Bioinformatics) doi:10.1007/978-3-642-02812-0_86.